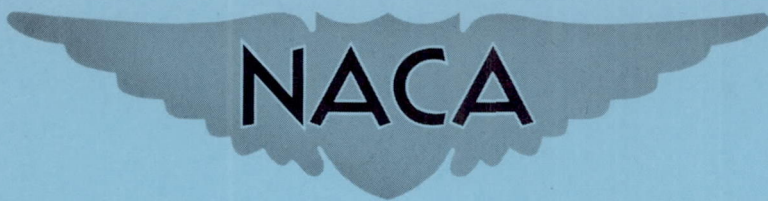RM L50G11

NACA

RESEARCH MEMORANDUM

LOW-SPEED STATIC STABILITY CHARACTERISTICS OF A

CANARD MODEL WITH A 45° SWEPTBACK WING AND A

60° TRIANGULAR HORIZONTAL CONTROL SURFACE

By John W. Draper

Langley Aeronautical Laboratory
Langley Air Force Base, Va.

NATIONAL ADVISORY COMMITTEE
FOR AERONAUTICS

WASHINGTON
September 6, 1950

NATIONAL ADVISORY COMMITTEE FOR AERONAUTICS

RESEARCH MEMORANDUM

LOW-SPEED STATIC STABILITY CHARACTERISTICS OF A

CANARD MODEL WITH A 45° SWEPTBACK WING AND A

60° TRIANGULAR HORIZONTAL CONTROL SURFACE

By John W. Draper

SUMMARY

An investigation has been made of the low-speed static stability characteristics of a canard model with a 45° sweptback wing and a 60° triangular horizontal control surface. The model had practically no allowable center-of-gravity range because of longitudinal instability that occurred at moderate and high lift coefficients with horizontal-control-surface incidences of 10° or less. The horizontal control surface produced a sidewash which, at an incidence of 15° and at angles of attack greater than 7°, was strong enough to make the model directionally stable with the vertical tail off. This sidewash caused a vertical tail mounted on the fuselage to be destabilizing at angles of attack above 11°. Twin vertical tails mounted at the wing tips did not produce a similar destabilizing effect because they were located outside the sidewash field.

INTRODUCTION

Interest in canard airplanes has recently been revived because the results of several studies have indicated that the canard appears promising for use at transonic and supersonic speeds (for example, reference 1). The National Advisory Committee for Aeronautics is making a general study of canard airplanes and results of several investigations are presented in references 1 to 5. As part of this general study, an investigation has been made in the Langley free-flight tunnel to determine the low-speed static stability and control characteristics of a canard model. The configuration tested was similar to that of references 1 to 3 and had a circular-cross-section fuselage with a fineness ratio of 13.5, an untapered 45° sweptback wing with aspect ratio 4.1, an untapered 45° sweptback vertical tail at the extreme rear of the fuselage, and a 60° triangular horizontal control surface at the nose.

The present investigation consisted of force tests to determine the longitudinal and lateral stability characteristics of the complete model and of various combinations of the fuselage, wing, vertical tail, and horizontal control surface. Tests were also made to determine the effects on the lateral stability of several changes in the horizontal control surface and vertical-tail configurations.

SYMBOLS AND COEFFICIENTS

All forces and moments are measured about the stability axes which are defined in figure 1.

C_L lift coefficient (Lift/qS)

C_D drag coefficient (Drag/qS)

C_m pitching-moment coefficient (Pitching moment/$qS\bar{c}$)

C_l rolling-moment coefficient (Rolling moment/qSb)

C_Y lateral-force coefficient (Lateral force/qS)

C_n yawing-moment coefficient (Yawing moment/qSb)

q dynamic pressure, pounds per square foot $\left(\frac{1}{2}\rho V^2\right)$

ρ air density, slugs per cubic foot

V airspeed, feet per second

S wing area, square feet

b wing span, feet

$\bar{c}$ mean aerodynamic chord of the wing, feet

α angle of attack of fuselage center line, degrees

ψ angle of yaw, degrees

β angle of sideslip, degrees $(-\psi)$

$C_{n\beta}$ rate of change of yawing-moment coefficient with angle of sideslip in degrees $\left(\partial C_n/\partial\beta\right)$

C_{l_β} rate of change of rolling-moment coefficient with angle of sideslip in degrees $\left(\partial C_l / \partial \beta\right)$

C_{Y_β} rate of change of lateral-force coefficient with angle of sideslip in degrees $\left(\partial C_Y / \partial \beta\right)$

i_t incidence of horizontal control surface (positive with leading edge up), degrees

b_t span of horizontal control surface, feet

h_t height of horizontal control surface above fuselage center line, feet

y_t lateral location of center line of horizontal control surface (measured from fuselage center line), feet

Model designations:

F   fuselage

W   wing

V   vertical tail

H   horizontal control surface

(H)   horizontal control surface in position but not attached to model

Subscripts:

E   twin vertical tails located on wing tips

0,5,10   angle of incidence of horizontal control surface, degrees

R   rectangular-plan-form horizontal control surface

APPARATUS AND MODEL

The force tests to determine the static aerodynamic characteristics of the model were made on the six-component balance of the Langley free-flight tunnel described in reference 6.

A three-view drawing and a photograph of the model used in the investigation are given as figures 2 and 3, respectively. Dimensional

characteristics of the model are presented in table I. The model was
constructed of hardwood and balsa with no movable surfaces other than
the horizontal control surface. No appreciable gap was formed between
the horizontal control surface and fuselage when the surface was deflected.
The wing and the single vertical tail had an NACA 65-009 airfoil section
normal to the leading edge (6.35 percent thick parallel to air stream)
while the triangular horizontal control surface was a $\frac{1}{4}$- inch-thick flat
plate with a rounded leading edge and tapered trailing edge. The results
obtained with the flat-plate airfoil section used on the model are
approximately the same as would have been obtained with a conventional
section because the aerodynamic characteristics of delta wings are vir-
tually independent of the airfoil section at low scale. This character-
istic has been established by comparison of the aerodynamic character-
istics of some flat-plate delta wings from reference 7 with those of
some German data on delta wings (reference 8) having NACA 0012 airfoil
sections and with those of some unpublished data on a 60° delta wing
with an NACA 0015-64 airfoil section. The twin vertical tails and rec-
tangular horizontal control surface used in the investigation were flat
plates. It was assumed that the results obtained with these flat-plate
surfaces would be comparable to those obtained with conventional sections
at low scale.

TESTS

Tests were made to determine the static longitudinal stability char-
acteristics of the model over an angle-of-attack range. Lateral stability
characteristics were determined over the angle-of-attack and angle-of-yaw
ranges. Table II is an index which shows the combinations of the model
components tested.

The lateral stability characteristics were determined in two ways.
An indication of the variation of the lateral stability characteristics
with angle of attack was obtained by determining the static lateral
derivatives from the slope of the curves between the coefficients meas-
ured at angles of yaw of ±5°. The lateral-stability coefficients were
also determined from tests over a range of yaw angles from 20° to -20°
for various angles of attack. For the case for which the variation of
lateral coefficients with angle of yaw is nonlinear, the plots of
lateral coefficients against angle of yaw give a better indication of
the lateral stability of the model than the plots of the lateral-stability
derivatives against angle of attack.

All tests were run at a dynamic pressure of 4.1 pounds per square
foot, which corresponds to an airspeed of about 40 miles per hour at

standard sea-level conditions and to a Reynolds number of 3.2×10^5 based on the mean aerodynamic chord of the wing of 0.85 foot. All longitudinal data for the model are referred to a center-of-gravity position of 0.80 mean aerodynamic chord ahead of the leading edge of the mean aerodynamic chord of the wing unless otherwise noted. A center-of-gravity position of 0.56 mean aerodynamic chord ahead of the leading edge of the mean aerodynamic chord was used for all lateral data. The vertical position of the center of gravity was assumed to be the fuselage center line for all tests.

For some tests, streamers of string approximately 6 inches long were attached at various locations along the fuselage in order to permit observation of the direction of flow over the fuselage. These studies were made under the same conditions as the force tests.

RESULTS AND DISCUSSION

The results of force tests made to determine the static longitudinal and lateral stability characteristics of the model are presented in figures 4 to 24. Table II is an index to these figures and a key to the configurations tested.

Longitudinal Stability and Control

The results of the tests made with various incidence settings of the horizontal control surface are presented in figure 4. These results show that the model becomes unstable at a lift coefficient of about 0.9 with control-surface incidences of 0°, 5°, and 10° for a center-of-gravity position of 0.80 mean aerodynamic chord ahead of the mean aerochord; with horizontal-control-surface incidences of 15° and 20°, a stable pitching moment is obtained over the complete lift range because the horizontal control surface stalls at a lower angle of attack than the wing. The model also becomes unstable at a lift coefficient of about 0.9 with $i_t = 15^\circ$ when the center of gravity is moved rearward (fig. 5). The reason for the break in the pitching-moment curve is indicated by the curve for the horizontal control surface off in figure 4 and by figure 6 which presents the longitudinal characteristics of some of the component parts. The wing pitching-moment curve against angle of attack breaks upward, apparently because the wing lift-curve slope decreases and because the wing aerodynamic center is well behind the center of gravity. This point is illustrated more clearly by figure 7 in which the wing pitching-moment curve referred to the 0.25 mean aerodynamic chord is compared with the curve for 0.80 mean aerodynamic chord ahead of the mean-aerodynamic-chord position. When the data are presented about the wing quarter chord

the pitching-moment curve is approximately linear up to an angle of
attack of 24°. Evidence that the falling off of the lift-curve slope
is responsible for the break in the pitching-moment curve is given by
the dashed lines of figure 7 which represent the case where the lift
curve was assumed to be linear up to an angle of attack of 24°. If the
wing lift holds up (which would be expected at higher Reynolds number)
a linear pitching-moment curve is obtained. These results show that an
early change in the slope of the lift curve of the wing is particularly
undesirable for a canard airplane because the wing is well behind the
center of gravity. For a conventional airplane this effect is much
smaller (or perhaps, even in the opposite direction) because the center
of gravity is much farther back.

The variation with angle of attack of the incremental pitching
moment produced by the horizontal control surface at various incidences
is shown in figure 8. The angle of attack at which the slope of the
horizontal-control-surface-effectiveness curve begins to decrease is,
of course, dependent on the angle of incidence of the surface. The
horizontal-control-surface effectiveness remains essentially constant
up to an angle of attack of about 30° for incidences of 0° and 5°. At
tail incidences of 10°, 15°, and 20° the slope of the horizontal-control-
surface-effectiveness curve decreases at lower angles of attack because
of the decreasing lift-curve slope of the surface. This decrease in
lift-curve slope decreases the pitching moment of the horizontal surface
and tends to balance out the effect of the decrease in pitching moment
caused by the decrease in lift-curve slope of the wing (figs. 4 and 5).
If the lift-curve slopes of the wing and horizontal surface break at the
same time (and by the proper amount) the pitching-moment curve for the
complete model will tend to remain linear. For this model the isolated
horizontal control surface starts to stall at about 28° angle of attack
(reference 7) and the wing stalls at about 12° which is a difference
of 16° between the stall angles. Therefore, with the incidence of 15°,
the two effects should tend to balance out and give a more linear
pitching-moment curve than those obtained with the lower angle of inci-
dence. The data of figures 4 and 5 show that this is the case.

The allowable center-of-gravity range can be defined as the dis-
tance from the most rearward center-of-gravity location for which the
model is at least neutrally stable in the trimmed condition to the most
forward center-of-gravity location at which the model can trim to the
maximum lift coefficient with horizontal control surface ($C_L = 1.1$).
On this basis the model had practically no allowable center-of-gravity
range because of the longitudinal instability that occurred at moderate
and high lift coefficients with incidences of 10° or less (fig. 5).
Canard designs which have a stable wing pitching moment and a horizontal
control surface which stalls at the same time as the wing would probably
have a somewhat greater center-of-gravity range.

Lateral Stability and Control

The results of lateral-stability force tests of the complete model are presented in figures 9 and 10. The data of figure 9 are presented in the form of lateral-stability derivatives which were obtained by measuring the forces and moments at $\pm 5^{\circ}$ yaw and by assuming a linear variation of the lateral coefficients between $\pm 5^{\circ}$. The data of figure 10 show the variation of the lateral coefficients with angle of yaw and indicate that the variation between $\pm 5^{\circ}$ yaw is not linear for all conditions. Therefore, the results obtained from the tests of angle of yaw of $\pm 5^{\circ}$ should be used only as qualitative data. Absolute values of the lateral-stability derivatives should be measured from the curves of lateral coefficients plotted against angle of yaw.

The results of figures 9 and 10 show that, for a horizontal-control-surface incidence of 0°, the directional stability derivative C_{n_β} decreased with increasing angle of attack. These results also show that an increase in tail incidence caused an increase in C_{n_β} as well as in the effective dihedral derivative $-C_{l_\beta}$ and resulted in a change in sign of the lateral-force derivative $-C_{Y_\beta}$ at moderate and high angles of attack.

The variation of the lateral-stability derivatives with angle of attack for a center-of-gravity position within the allowable center-of-gravity range (0.70 M.A.C. ahead of the leading edge of the mean aerodynamic chord) and with the horizontal control surface set at the proper position for trim is shown in figure 11. These results show that the model is directionally stable over the angle-of-attack range under these conditions.

Presented in figures 12 to 16 are the results of tests made of various components individually and in combinations in an effort to explain these effects of horizontal-control-surface incidence on the lateral stability. The results of figures 12 and 14(a) show that the lateral characteristics of configuration FWV are normal for such an arrangement. With the addition of the horizontal control surface at 0° incidence, however, (configuration FWVH$_0$) there is a rapid reduction in C_{n_β} and $-C_{Y_\beta}$ with increasing angle of attack in the moderate to high angle-of-attack range and an increase in $-C_{l_\beta}$ at the moderate angles. On the other hand, tests made with the vertical tail off (FWH$_0$ and FWH$_{15}$ on figs. 13 and 14(b)) show that the horizontal control surface with 0° incidence had a small stabilizing effect $\left(\text{increased } C_{n_\beta}\right)$ at higher angles of attack, and with 15° incidence had such a large stabilizing effect that it resulted in the model with vertical tail off being directionally stable above an angle of attack of 7°. Tests made of the

combination of fuselage and horizontal control surface $\left(FH_0 \text{ and } FH_{15} \text{ on}\right.$
fig. 15$\left.\right)$ showed a similar effect of the tail to that shown by the data
of figures 13 and 14 for the configurations $\left(FWH_0 \text{ and } FWH_{15}\right)$. The results
of tests made to determine the variation of C_{n_β} at the higher angles of
attack for configurations FWH_{15} and $FWVH_{15}$ are presented in figure 16.
These results show a rapid increase in C_{n_β} for both configurations at
the higher angles of attack. The results of figures 12 to 16 indicate
that the horizontal control surface with $i_t = 15^\circ$ causes the vertical
tail to be directionally destabilizing above an angle of attack of 11°
and causes the fuselage to be directionally stable at moderate and high
angles of attack.

A more definite indication of the effect of the horizontal control
surface on the lateral stability is given in figure 17 where results of
tests of the configurations FW, H_{15}, FWH_{15}, and $FW\left(H_{15}\right)$ are presented.
The data for the H_{15} configuration were obtained by testing the isolated
horizontal control surface on a sting mounting and referring the forces
and moments to the center-of-gravity position for the complete model.
The $FW\left(H_{15}\right)$ results were obtained with the surface in position with
respect to the fuselage but without the surface being supported by the
fuselage. These results show that the horizontal control surface alone
and the wing-fuselage combination are unstable. When the horizontal
control surface and wing fuselage are combined, however, the resulting
configuration is stable above 7° angle of attack. With the horizontal
control surface in its normal position but not attached to the model,
approximately the same stabilizing effect is obtained as that with the
control surface attached when tested at 20° angle of attack. The results
of these tests indicate that the stabilizing effect of the horizontal
control surface is not caused by the forces on the surface but is caused
by the influence of the surface on the flow field about the model.

The results of tuft surveys made to obtain a physical picture of the
flow field about the model at small angles of yaw are illustrated sche-
matically in figure 18. These studies showed that at 0° angle of attack
the streamers trailed essentially parallel to the air stream when the
model was yawed. At 16° angle of attack, however, the streamers did
not trail parallel to the air stream when the model was yawed but
trailed across the fuselage in the opposite direction indicating that
there was an effective reversal in the angle of sideslip of the model
caused by a sidewash from the horizontal control surface. This change
in the direction of flow over the fuselage came about gradually as the
angle of attack was increased.

Effect of vertical position of horizontal control surface.- Pre-
sented in figures 19 and 20 are the results of a series of tests made

with the horizontal control surface at several different vertical posi-
tions in an effort to determine the vertical location of the sidewash
field. Figure 19 shows that at 0° angle of attack the horizontal con-
trol surface $\left(i_t = 15°\right)$ was destabilizing $\left(\text{decreased } C_{n_\beta}\right)$ when it was
located on the fuselage center line but was stabilizing when it was
located 0.25 control-surface span above the center line. At 20° angle
of attack, the surface was stabilizing in both positions with the
greatest effect occurring with the surface on the center line. When the
surface was located 0.50 horizontal-control-surface span above the fuse-
lage center line the effect of the surface was relatively small at all
angles of attack; this small effect indicates that the sidewash was
missing the fuselage. Figure 20 is a summary of the effect of the surface
with $i_t = 15°$ at 0° angle of attack which shows that the greatest
effect occurs when the surface is located about 0.125 span above the
center line. These results indicate that the sidewash field has a slight
downward inclination. As the angle of attack is increased, more of the
fuselage becomes immersed in the sidewash field and a greater stabi-
lizing effect is obtained.

Effect of plan form of horizontal control surface.- In order to
determine whether the unusual sidewash characteristics were associated
only with a horizontal control surface with a triangular plan form, tests
using a surface of rectangular plan form with the same area and aspect
ratio as the triangular surface were made. These results are compared
with those for the triangular surface in figure 21 which shows that the
same effect exists to a limited extent for the rectangular surface. The
smaller effect of the rectangular surface is apparently caused partly
by the lower angle of attack at which it stalls. With 15° incidence
the break in the variation of C_{n_β} with angle of attack occurs at
16° angle of attack for the model with the triangular surface and at
8° angle of attack for the model with the rectangular surface. If
interference effects are neglected, these results might be taken to indi-
cate that the triangular surface stalls at about 31° angle of attack and
the rectangular surface stalls at about 23° angle of attack. These
stalling angles are in fairly good agreement with those shown in refer-
ence 7 for wings of similar plan form.

Effect of vertical-tail configuration.- The results of tests made
to determine whether twin vertical tails located at the wing tips would
be free of the influence of the horizontal control surface are presented
in figures 22 to 24. The data of figure 22 show that the twin vertical
tails provide approximately a constant increment of C_{n_β} over most of
the angle-of-attack range. Figures 23 and 24 show that the twin tails
give a linear variation of yawing moment with angle of yaw of about 15°;
this linear variation indicates that the tails are not influenced by
the sidewash field up to that angle of yaw.

Effect of horizontal control surface as a lateral-control device.-
When it was found that the sidewash created by the horizontal control
surface had a large effect on the lateral characteristics, tests were
made to determine whether this effect could be used to provide lateral
control. The results of these tests in which the horizontal control
surface was moved to several different lateral positions are presented
in figure 25. These results show that large yawing and rolling moments
were obtained at 15° angle of attack and 15° surface incidence. Moving
the surface to the left apparently caused a sidewash to the right which
gave positive values of lateral force and yawing moment. Large values
of rolling moment were produced because the horizontal-control-surface
lift was laterally displaced and because the wing was partly immersed
in the sidewash field. These results indicate that, in some flight
conditions, turning maneuvers might be executed by the lateral displace-
ment of the horizontal control surface.

CONCLUSIONS

The following conclusions were drawn from the results of the Langley
free-flight-tunnel investigation of the low-speed static stability char-
acteristics of a canard model having a 45° sweptback wing and vertical
tail and a 60° triangular-plan-form horizontal control surface.

1. The model had practically no allowable center-of-gravity range
because of longitudinal instability that occurred at moderate and high
lift coefficients with a horizontal-control-surface incidence of 10°
or less. This longitudinal instability was caused by a premature drop-
ping off of the wing lift-curve slope which was attributed, at least
partly, to the low scale of the tests.

2. The horizontal control surface produced a sidewash which made
the fuselage less directionally unstable and the vertical tail less
directionally stable as the angle of attack and angle of the horizontal
control surface were increased. At a horizontal-control-surface inci-
dence of 15°, the sidewash effect was strong enough to make the model
directionally stable with the vertical tail off at angles of attack
greater than 7° and to cause a vertical tail mounted on the fuselage to
be destabilizing at angles of attack above 11°. The results indicated
that, for a center-of-gravity position within the allowable center-of-
gravity range, the model would be directionally stable over the entire
lift range if the horizontal control surface was set at the proper

position for trim. Twin vertical tails mounted at the wing tips did not produce a destabilizing effect because they were located outside the sidewash field.

Langley Aeronautical Laboratory
    National Advisory Committee for Aeronautics
        Langley Air Force Base, Va.

REFERENCES

1. Mathews, Charles W.: Study of the Canard Configuration with Particular Reference to Transonic Flight Characteristics and Low-Speed Characteristics at High Lift. NACA RM L8G14, 1949.

2. Crane, Harold L., and Adams, James J.: Wing-Flow Measurements of Longitudinal Stability and Control Characteristics of a Canard Airplane Configuration with a 45° Sweptback Wing and a Triangular All-Movable Control Surface. NACA RM L50A31, 1950.

3. Kraft, Christopher C., Jr., and Mathews, Charles W.: Determination by the Free-Fall Method of the Drag and Longitudinal Stability and Control Characteristics of a Canard Model at Transonic Speeds. NACA RM L50D04, 1950.

4. Bates, William R.: Low-Speed Static Longitudinal Stability Characteristics of a Canard Model Having a 60° Triangular Wing and Horizontal Tail. NACA RM L9H17, 1949.

5. Bates, William R.: Low-Speed Lateral Stability Characteristics of a Canard Model Having a 60° Triangular Wing and Horizontal Tail. NACA RM L9J12, 1949.

6. Shortal, Joseph A., and Draper, John W.: Free-Flight-Tunnel Investigation of the Effect of the Fuselage Length and the Aspect Ratio and Size of the Vertical Tail on Lateral Stability and Control. NACA ARR 3D17, 1943.

7. Tosti, Louis P.: Low-Speed Static Stability and Damping-in-Roll Characteristics of Some Swept and Unswept Low-Aspect-Ratio Wings. NACA TN 1468, 1947.

8. Lange and Wacke: Test Report on Three- and Six-Component Measurements on a Series of Tapered Wings of Small Aspect Ratio (Partial Report: Triangular Wing). NACA TM 1176, 1948.

TABLE I

DIMENSIONAL CHARACTERISTICS OF THE CANARD MODEL

OF THE LANGLEY FREE-FLIGHT TUNNEL

Wing (W):
   Airfoil section . . . . NACA 65009
   Chord (normal to L.E), in. 7.20
   Span, in. 42.00
   Area, (including area covered by fuselage) sq ft 2.95
   Mean aerodynamic chord, in. 10.20
   Aspect ratio 4.1
   Sweepback (0.50c), deg 45.0
   Taper ratio 1.0
   Incidence, deg 0
   Dihedral, deg 0
   Twist, deg 0

Horizontal control surface (triangular) (H):
   Airfoil section . . . . Flat plate
   Root chord, in. 12.0
   Span, in. 12.0
   Area, (including area covered by fuselage) sq ft 0.50
   Mean aerodynamic chord, in. 6.0
   Aspect ratio 2.0
   Sweepback, (L.E.) 60.0
   Dihedral, deg 0
   Tail length (from L.E. M.A.C. wing to
     L.E. M.A.C. of tail), in. 47.25

Horizontal control surface (rectangular) (H_R):
   Airfoil section . . . . Flat plate
   Root chord, tip chord, in. 6.0
   Span, in. 12.0
   Area, (including area covered by fuselage) sq ft 0.50
   Mean aerodynamic chord, in. 6.0
   Aspect ratio 2.0
   Sweepback (L.E.) 0
   Dihedral, deg 0
   Tail length, (from L.E. M.A.C. wing to
     L.E. M.A.C. of tail), in. 46.65
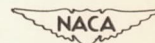
TABLE I

DIMENSIONAL CHARACTERISTICS OF THE CANARD MODEL

OF THE LANGLEY FREE-FLIGHT TUNNEL — Concluded

Vertical tail (V):
   Airfoil section . . . . NACA 65009
   Chord (normal to L.E.), in. 5.05
   Span, in. 10.70
   Area, (to fuselage center line), sq ft 0.53
   Aspect ratio 1.5
   Sweepback (0.50c), deg 45.0
   Taper ratio 1.0
   Tail length (from L.E. M.A.C. wing to
     L.E. M.A.C. of tail), in. 20.57

Twin vertical tails (V_E):
   Airfoil section . . . . Flat plate
   Chord (normal to L.E.), in. 6.20
   Span, in. 9.25
   Area, (total), sq ft 794
   Aspect ratio 1.5
   Sweepback (0.50c), deg 45.0
   Taper ratio 1.0
   Tail length (from L.E. M.A.C. wing to
     L.E. M.A.C. of tail), in. 12.02
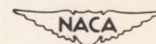
TABLE II

INDEX TO TESTS

Type of test	Configuration[1]	Figure
Longitudinal	F	6
	W	6 and 7
	FW	6
	FWV	4
	$FWVH_0$	4,5, and 6
	$FWVH_5$	4 and 5
	$FWVH_{10}$	4 and 5
	$FWVH_{15}$	4 and 5
	$FWVH_{20}$	4
Lateral	F	11,12, and 14
	H_{15}	16
	W	11
	FW	11,12,14,16, and 18
	FV	14
	FH_0	14
	FH_{15}	14
	FWV	11,12, and 13(a)
	FWH_0	12
	FWH_{15}	12,13(b),15,16,18,19,20,21, and 24
	FWH_{R15}	20
	$FW(H_{15})$	16
	$FWVH_0$	9,10(a), and 11
	$FWVH_{10}$	9
	$FWVH_{15}$	9,10(b),15,21, and 22
	FWV_EH_{15}	21 and 22
Tuft tests	$FWVH_{15}$	17

[1] The configurations are denoted by: F, fuselage; W, wing; V, vertical tail; H, horizontal control surface; subscript numbers indicate control-surface incidence measured in degrees. Subscript R indicates rectangular tail. Subscript E indicates twin tails. Parentheses around (H_{15}) indicate horizontal control surface in position but not attached to fuselage.
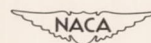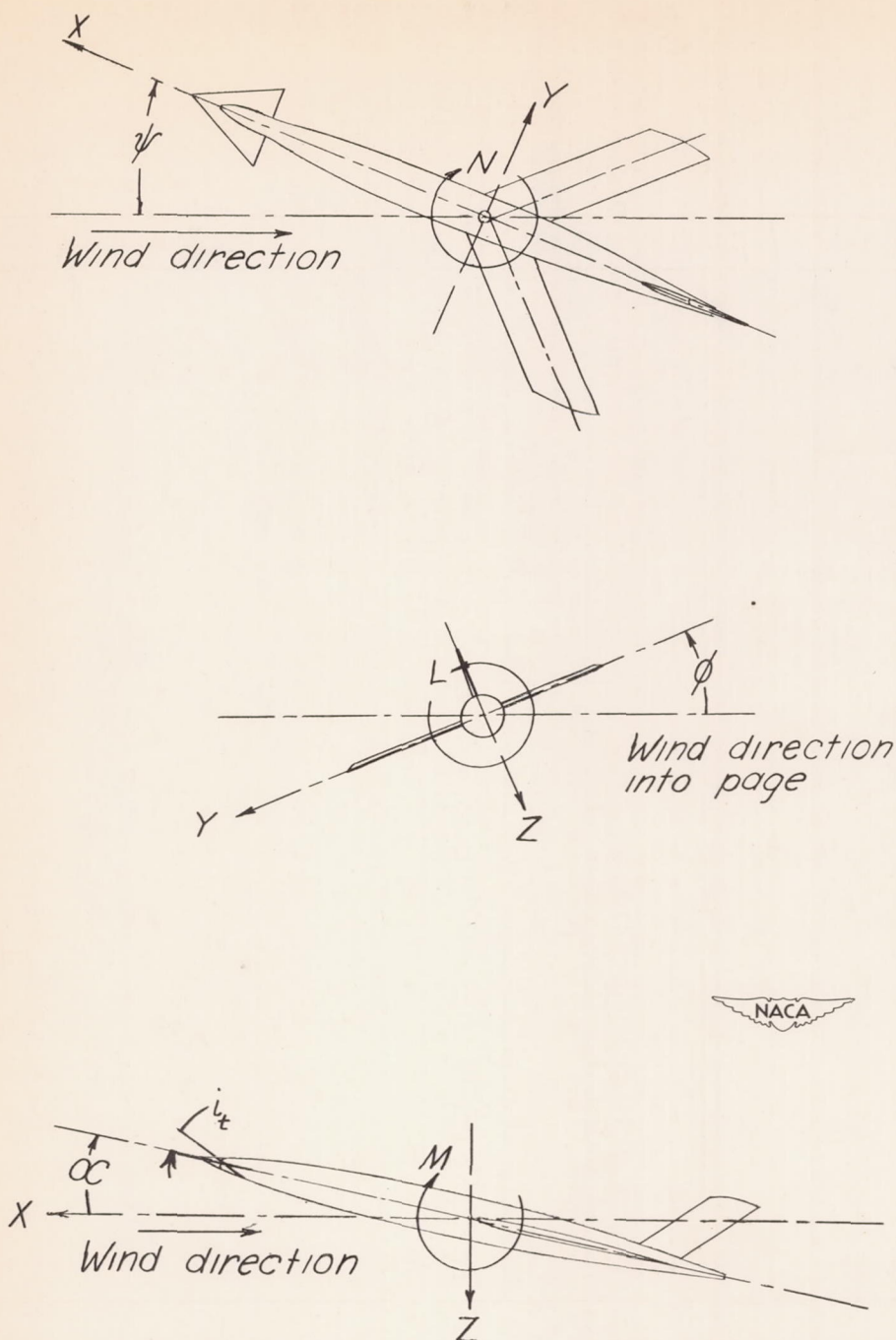
Figure 1.- The stability system of axes. Arrows indicate positive
   directions of moments, forces, and control-surface deflections.
   This system of axes is defined as an orthogonal system having
   their origin at the center of gravity and in which the Z-axis is
   in the plane of symmetry and perpendicular to the relative wind,
   the X-axis is in the plane of symmetry and perpendicular to the
   Z-axis, and the Y-axis is perpendicular to the plane of symmetry.
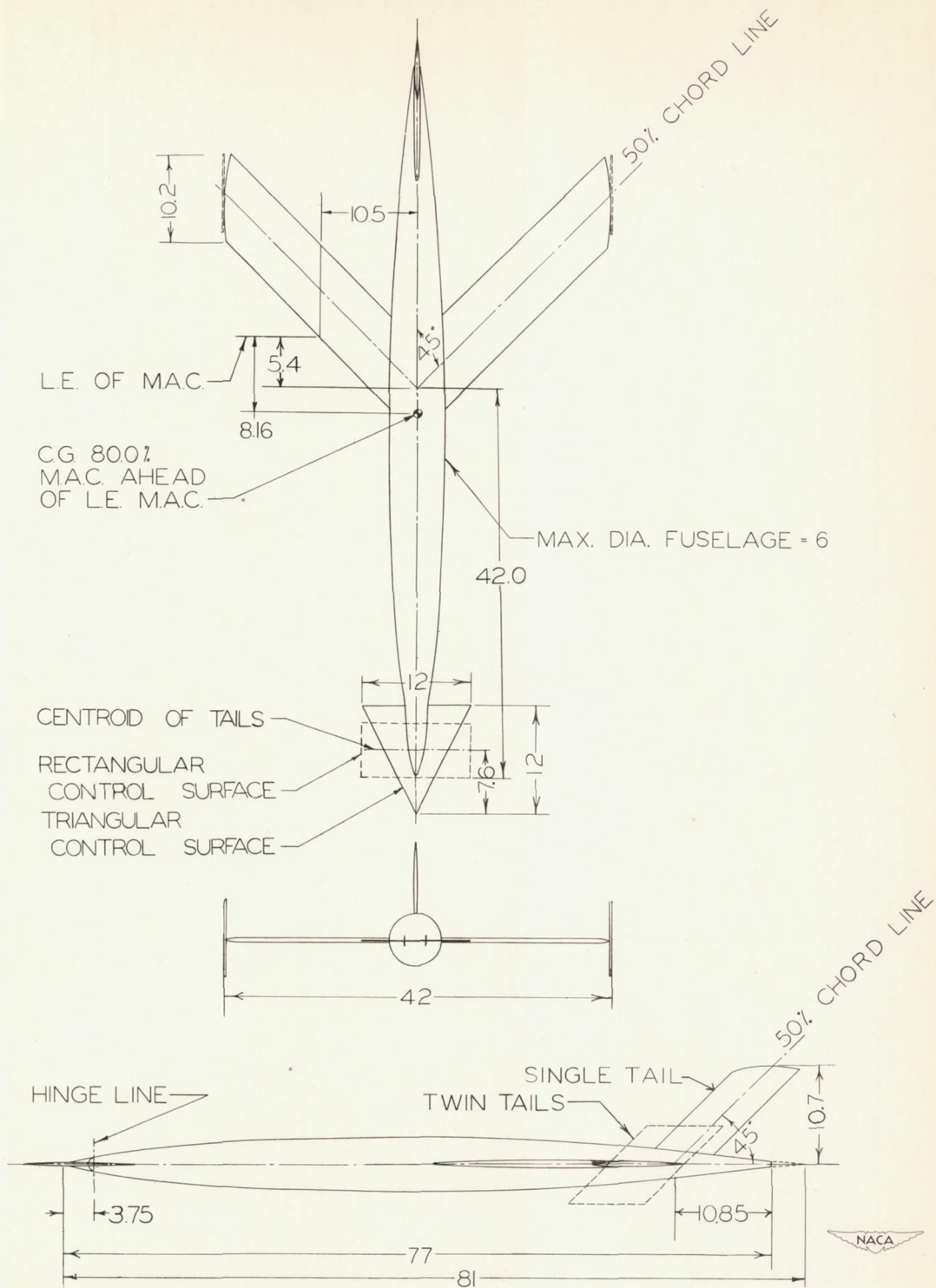
Figure 2.- Three-view drawing of model showing the various horizontal
control surfaces and vertical-tail configurations. All dimensions
are in inches.
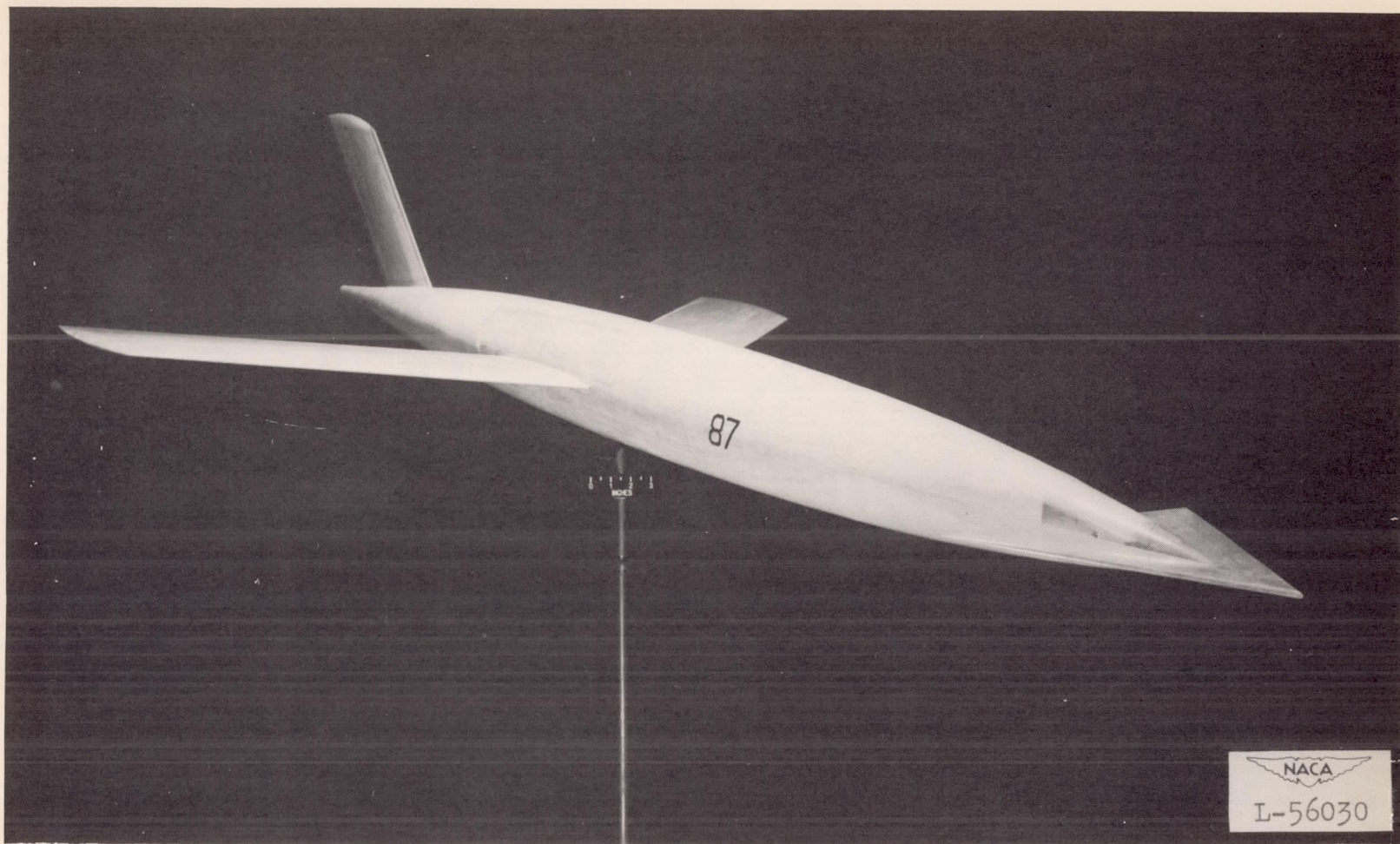
Figure 3.- Langley free-flight-tunnel canard model used in the
investigation.
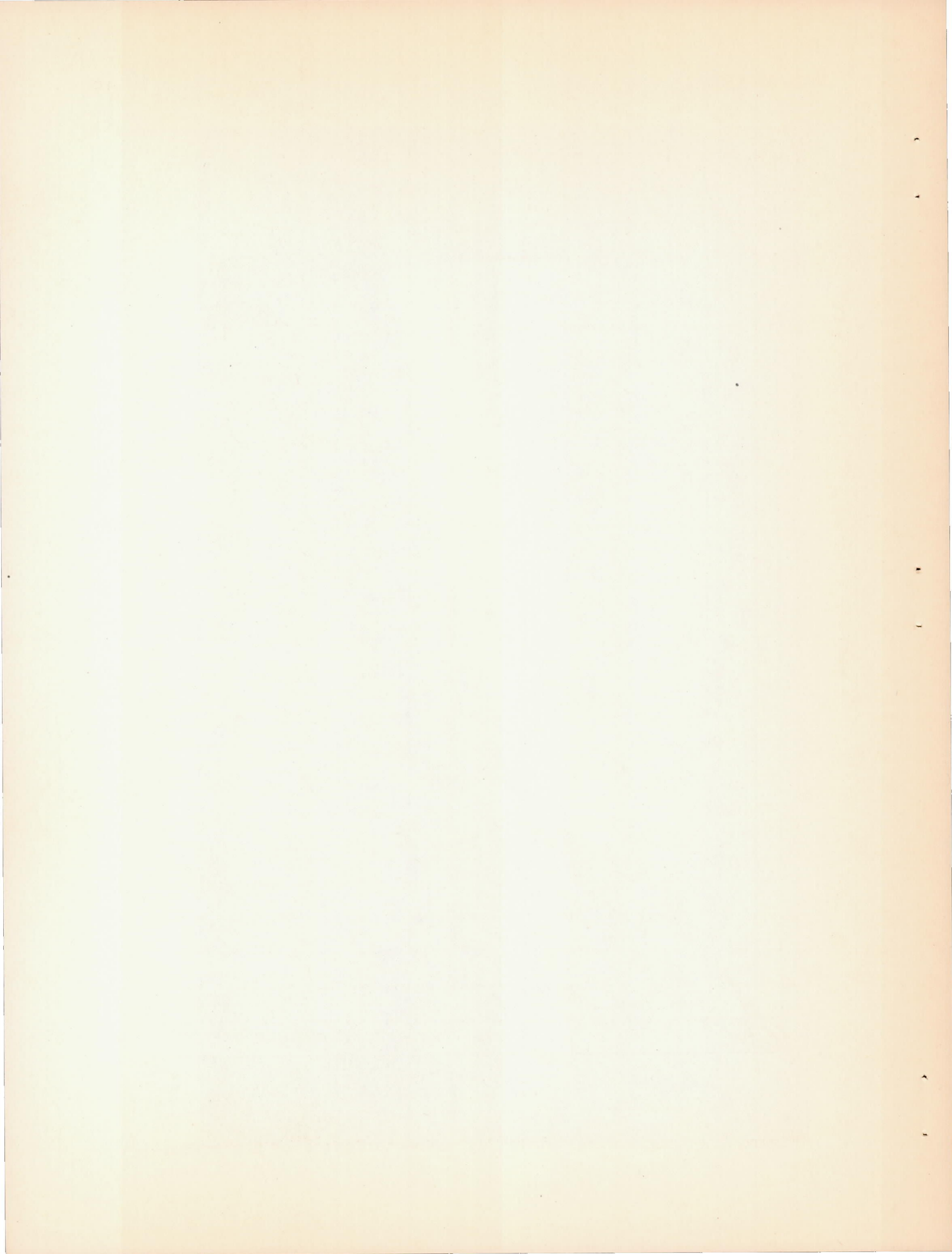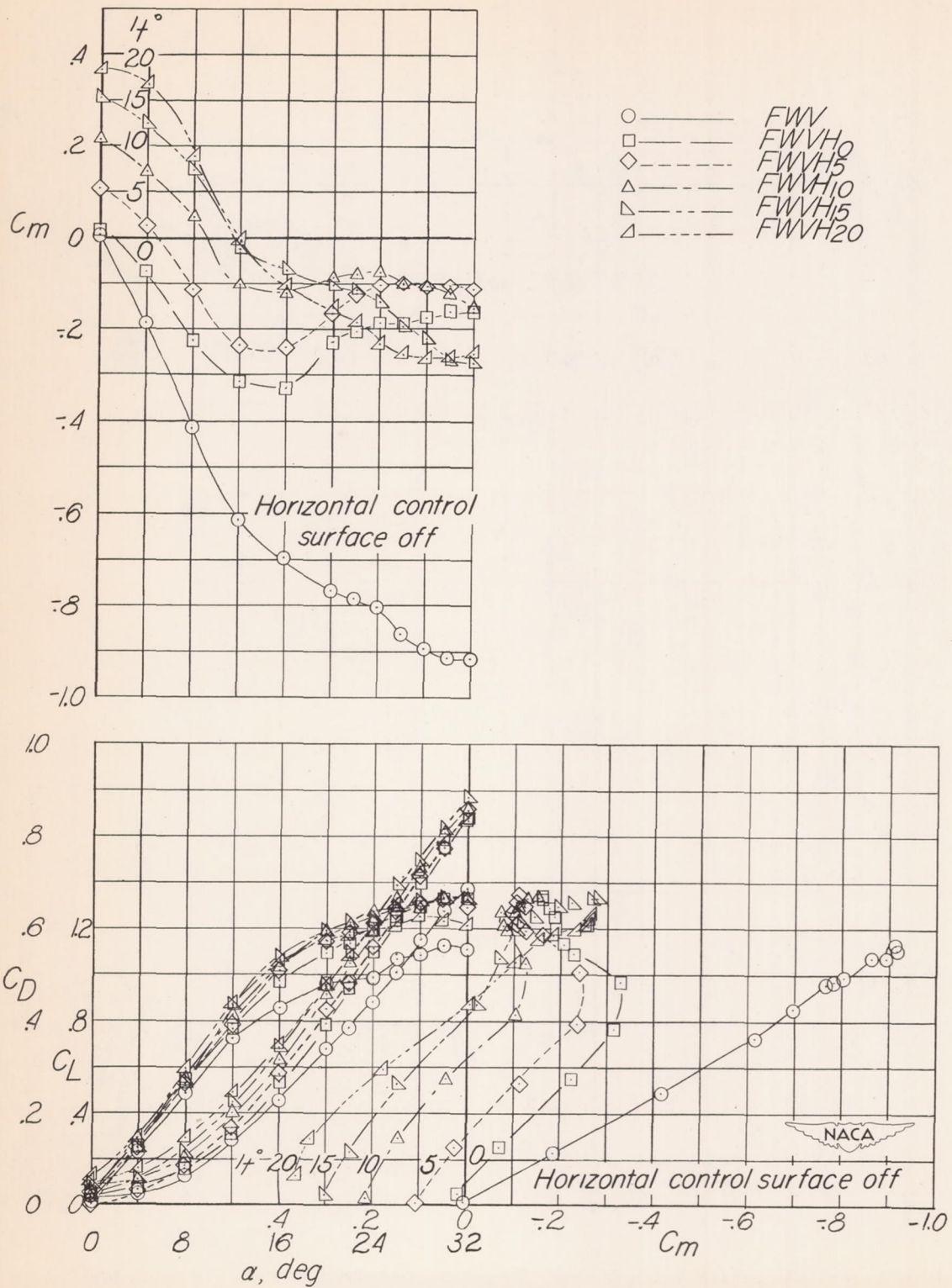
Figure 4.- Longitudinal stability characteristics of the model.
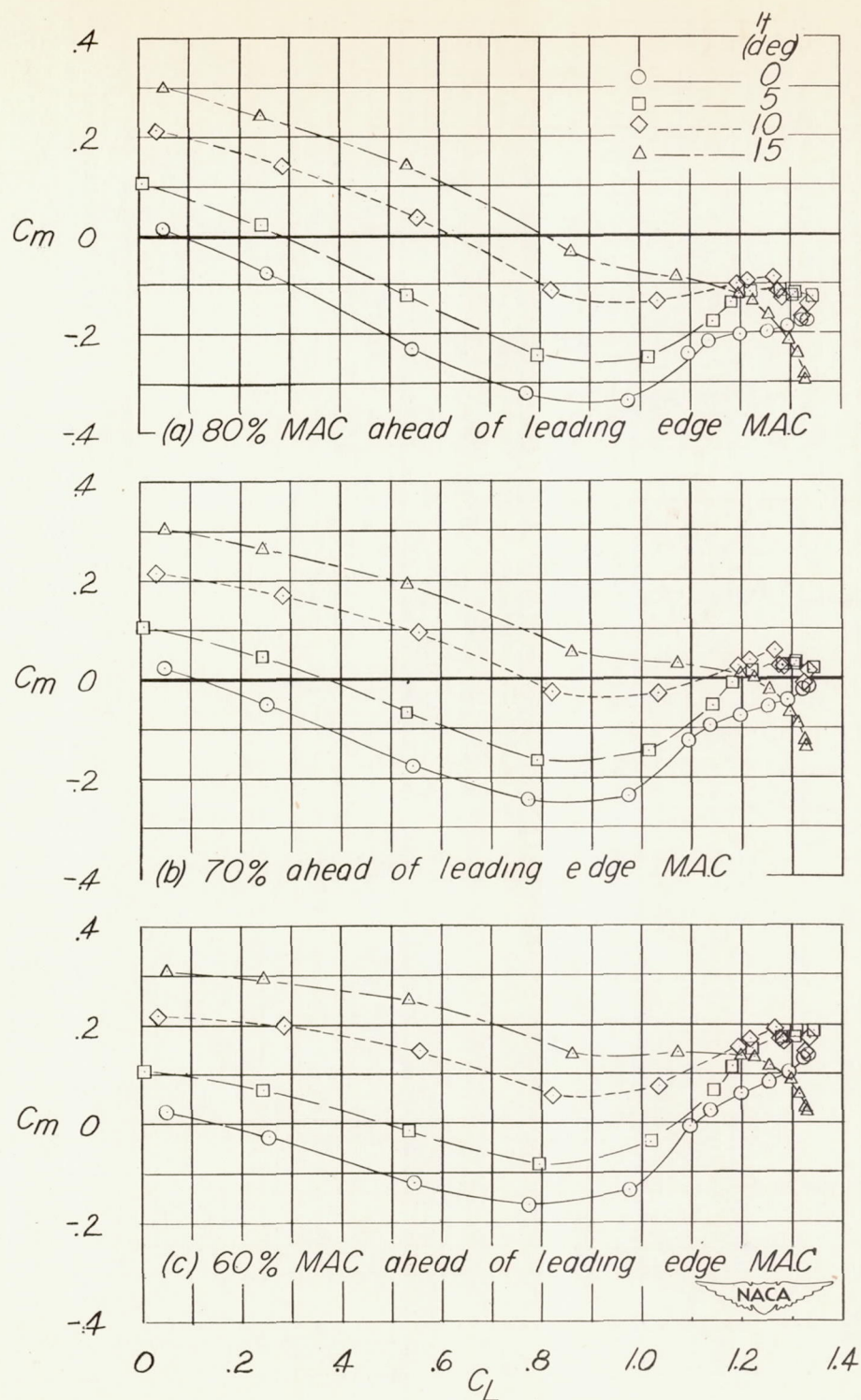
Figure 5.- The effect of horizontal-control-surface incidence and center-of-gravity location on the longitudinal stability and trim characteristics of the model.
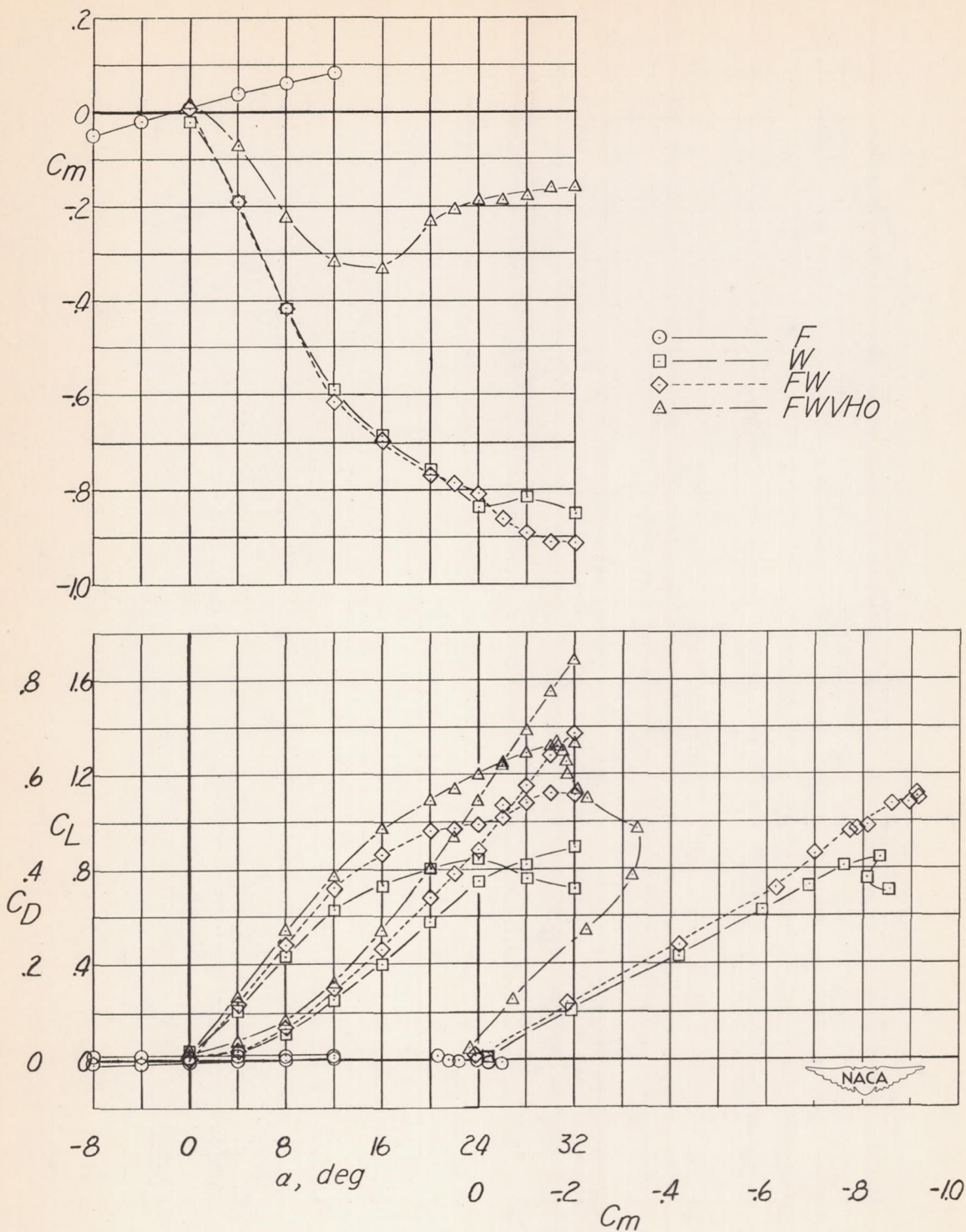
Figure 6.- Longitudinal stability characteristics of components of the model.
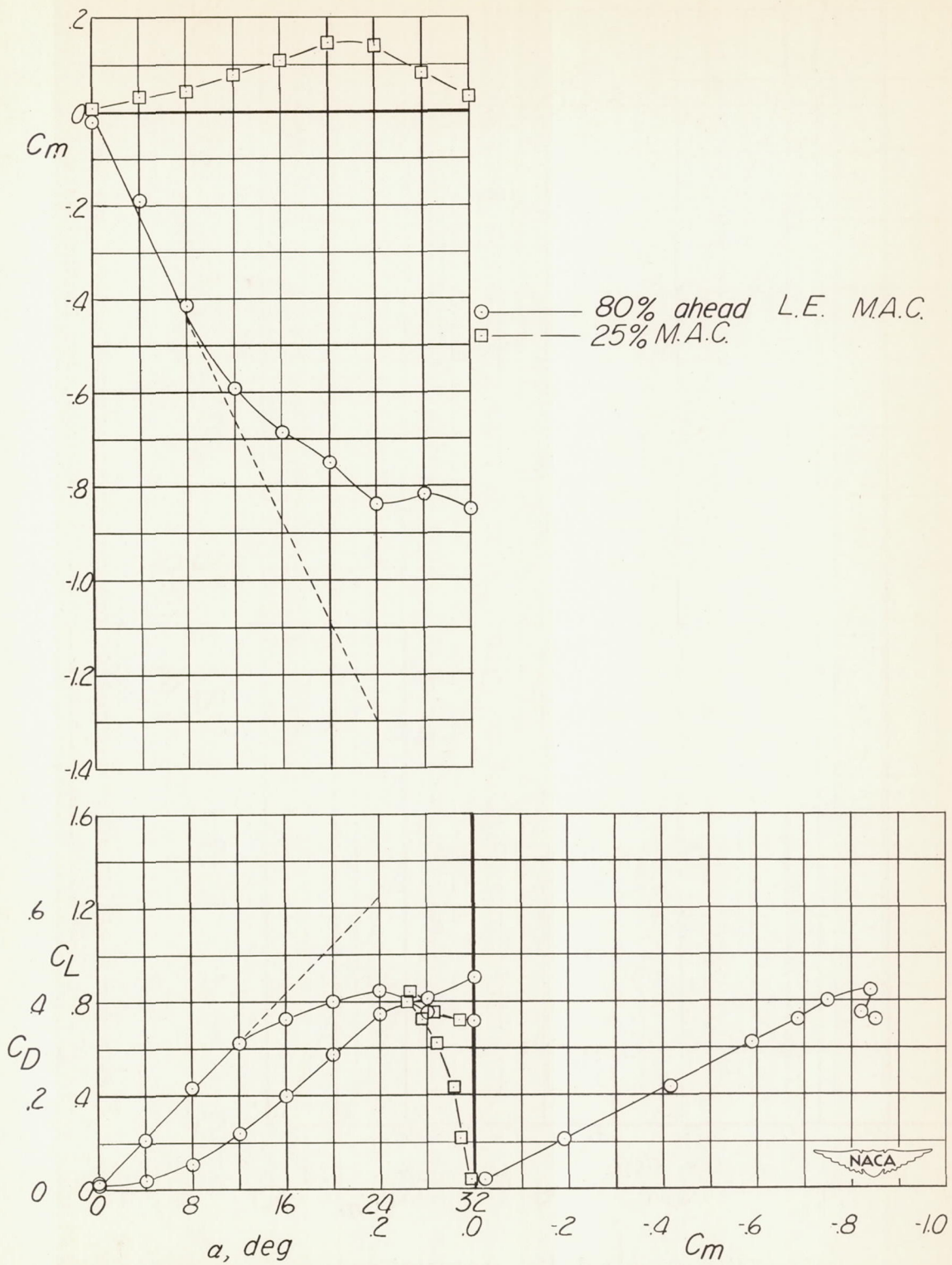
Figure 7.- Comparison of longitudinal stability characteristics of wing
alone at two center-of-gravity locations.
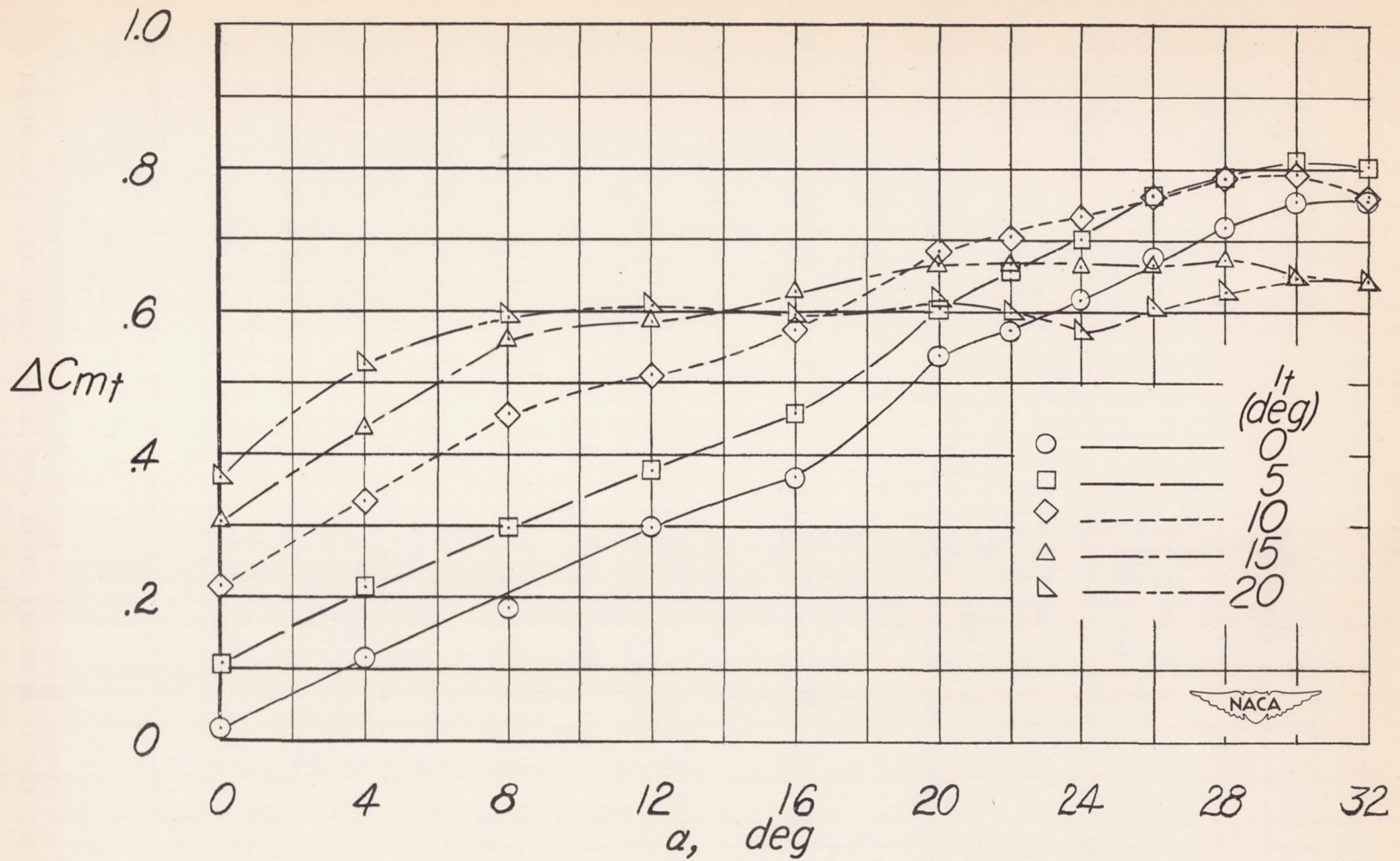
Figure 8.- Pitching effectiveness of triangular horizontal control surface
for the various horizontal-control-surface settings used in the tests
of the model.
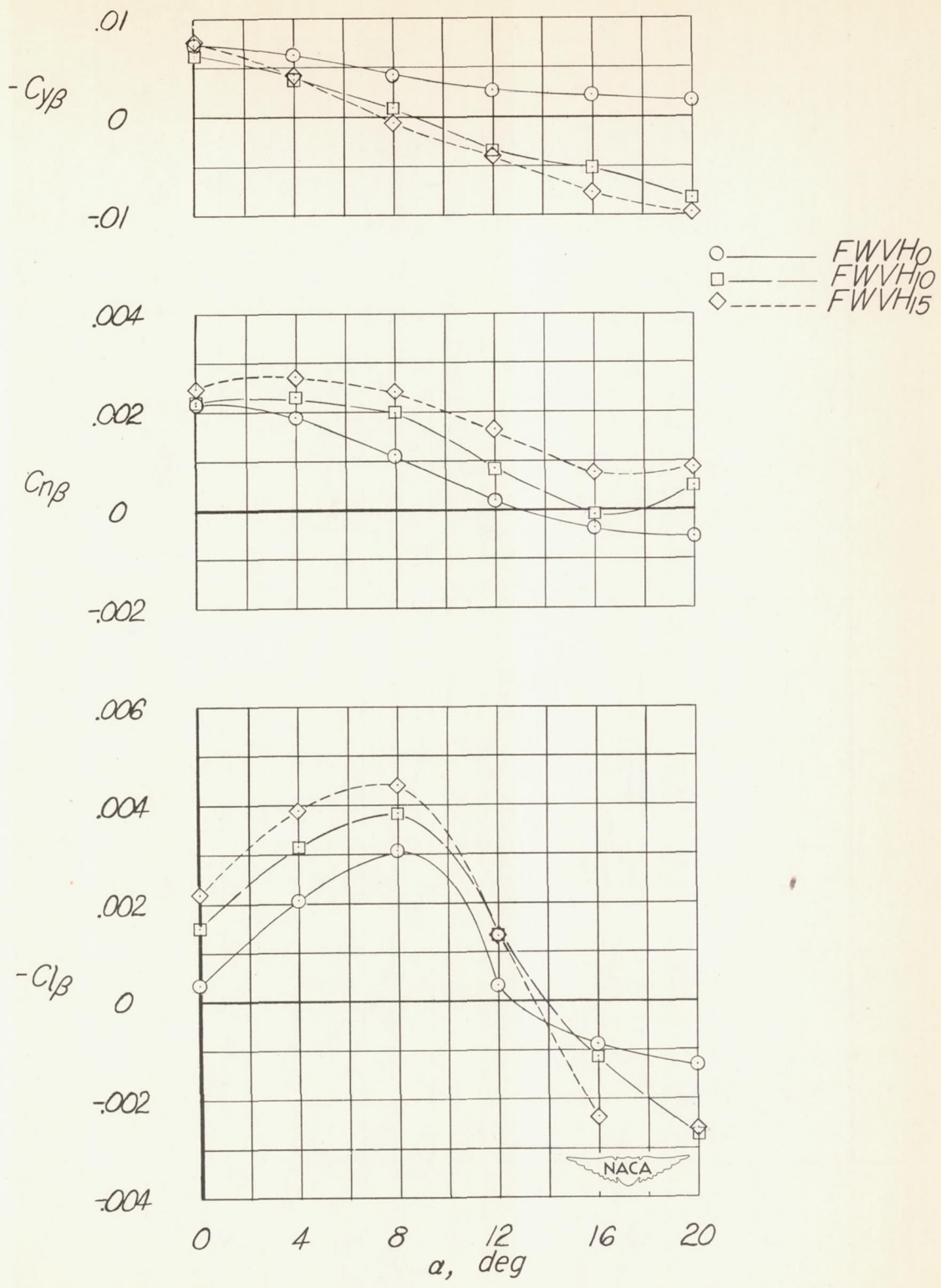
Figure 9.- Lateral stability characteristics of the model with various incidence settings of the horizontal control surface.
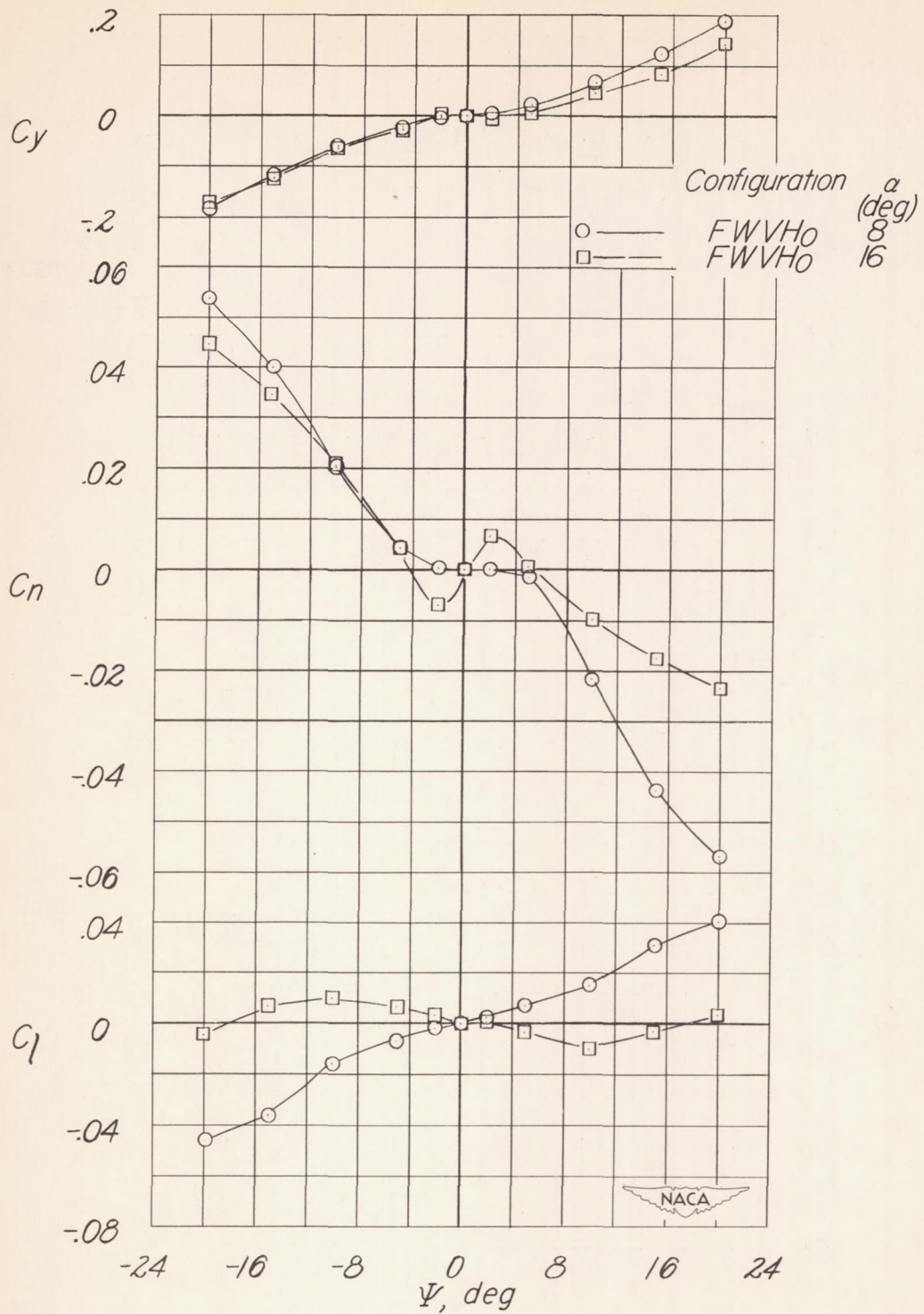
(a) Complete model configuration. $i_t = 0°$.

Figure 10.- Lateral characteristics of the model.
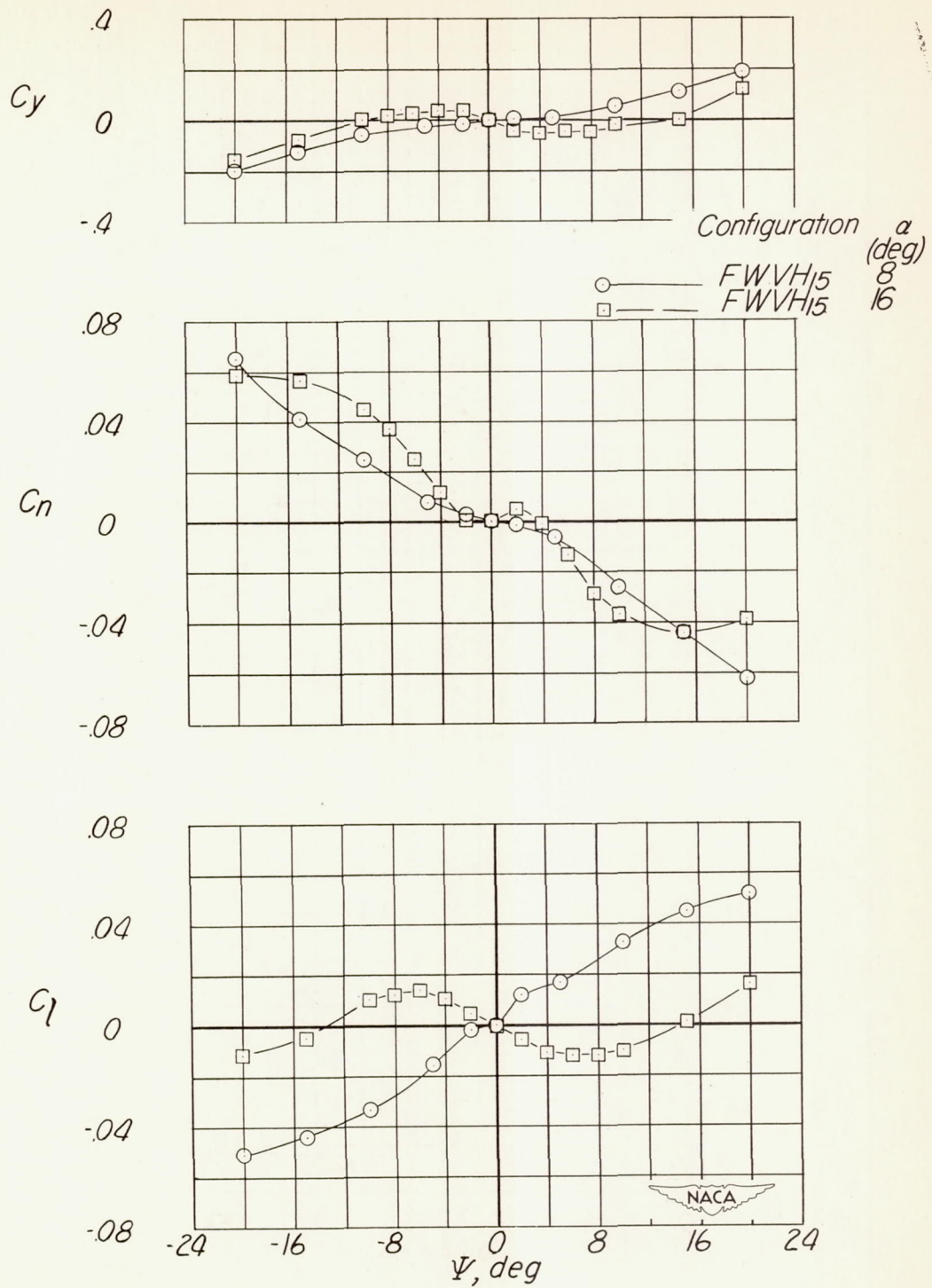
(b) Complete model configuration. $i_t = 15°$.

Figure 10.- Concluded.
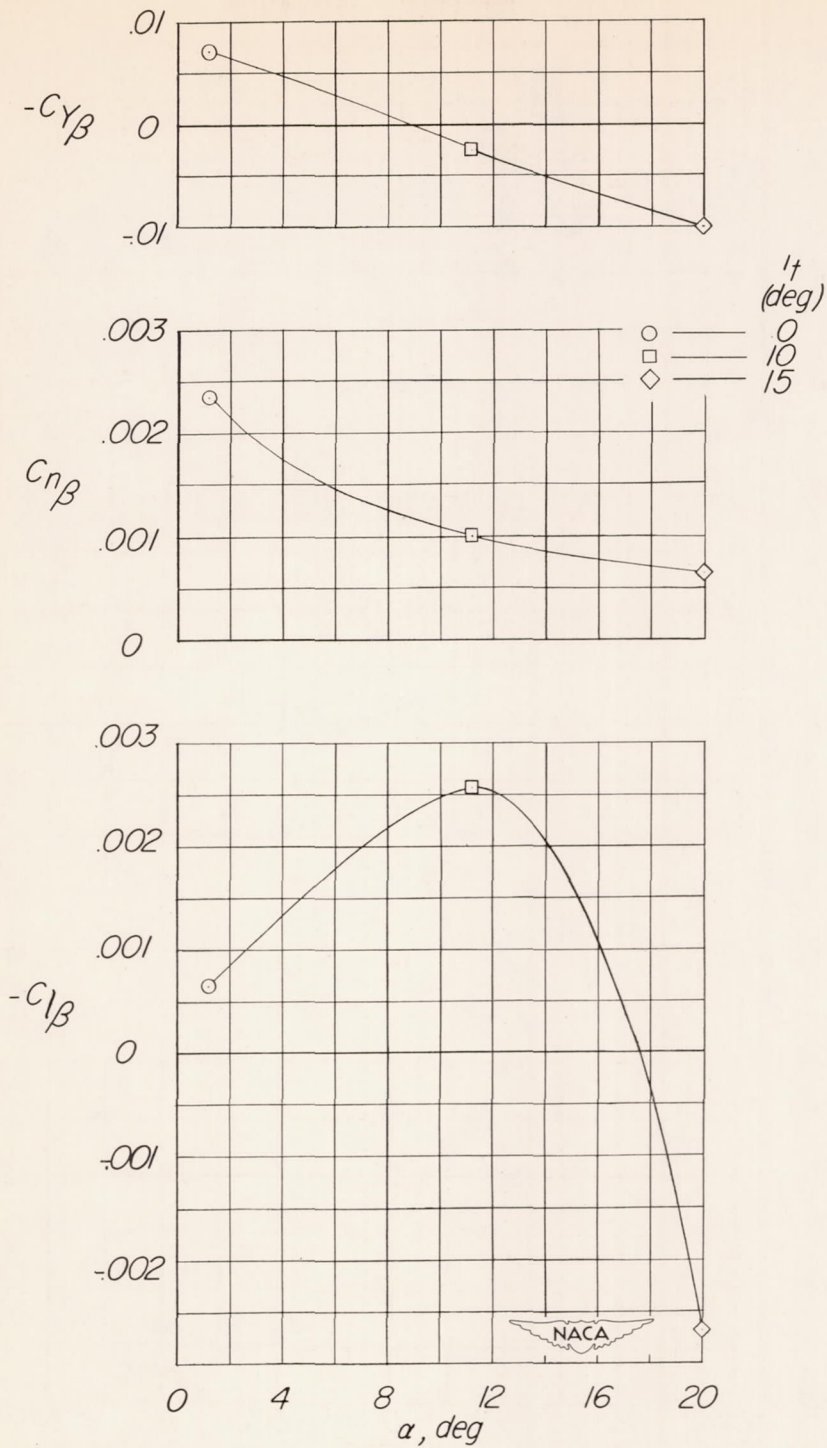
Figure 11.- Variation of lateral-stability derivatives with angle of
attack for trim conditions of configuration FWVH with the center of
gravity 0.70 mean aerodynamic chord ahead of the leading edge of the
mean aerodynamic chord.
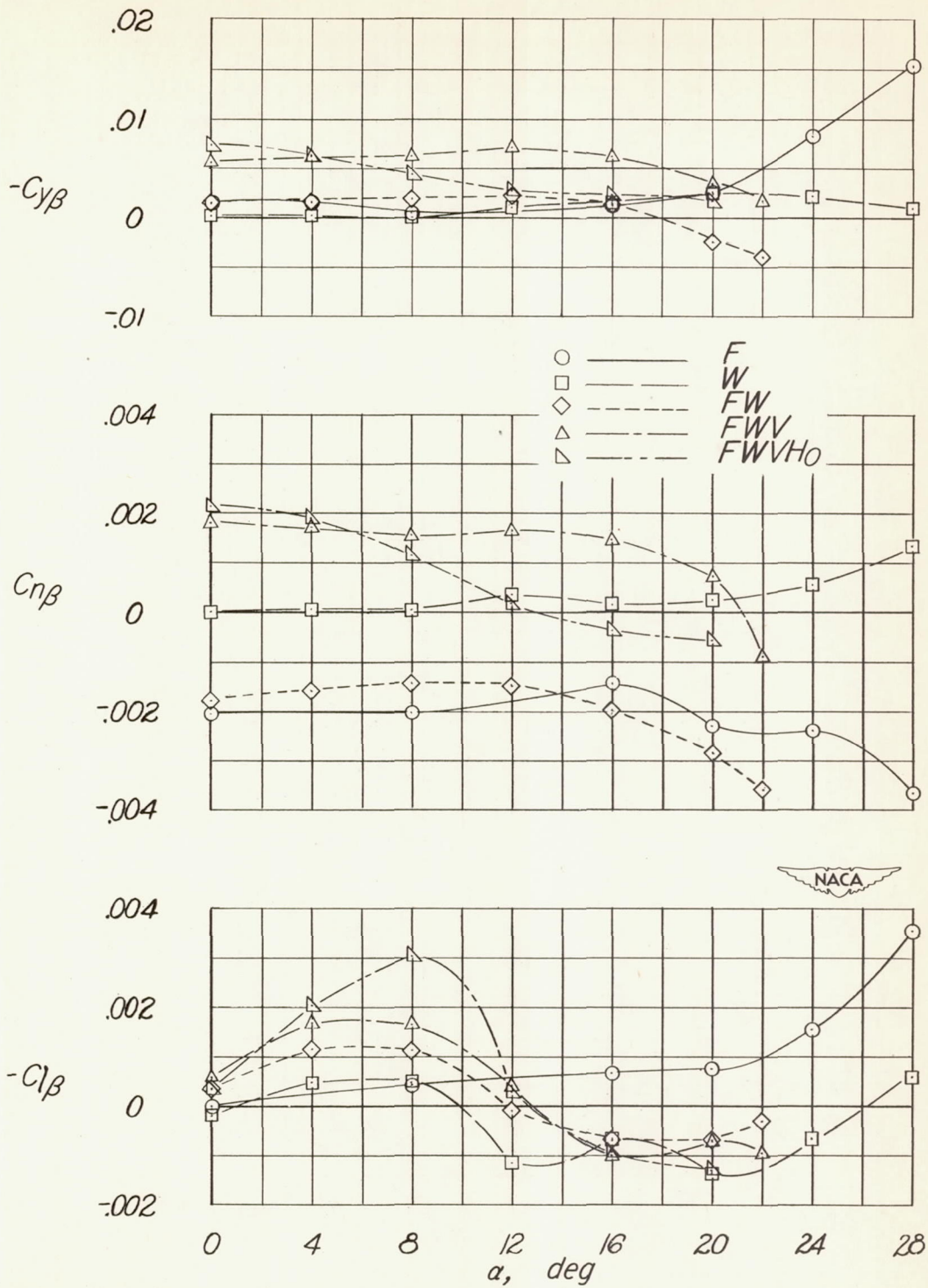
Figure 12.- Lateral stability characteristics of components of the model.
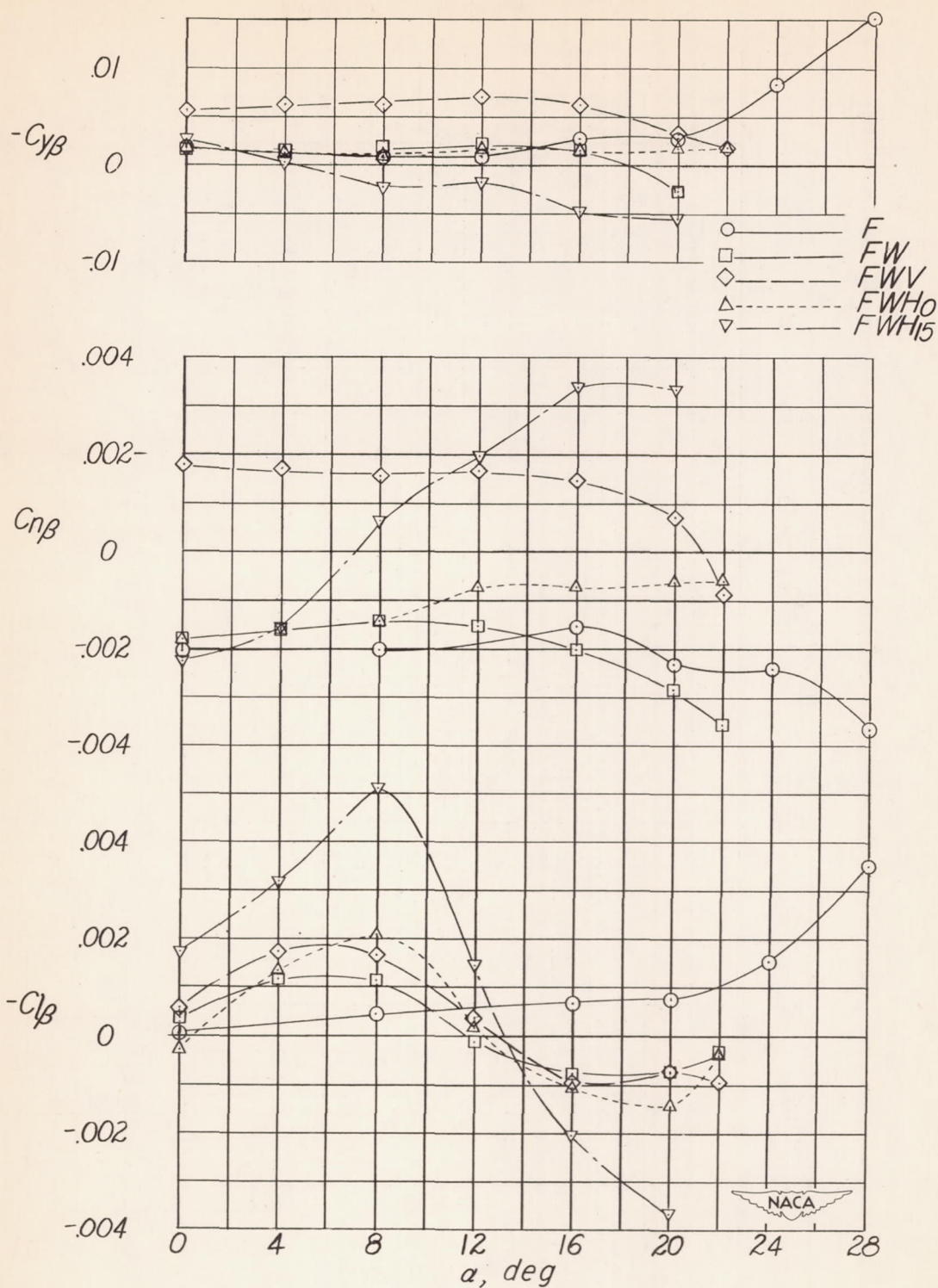
Figure 13.- Lateral stability characteristics of combinations of components
of the model.
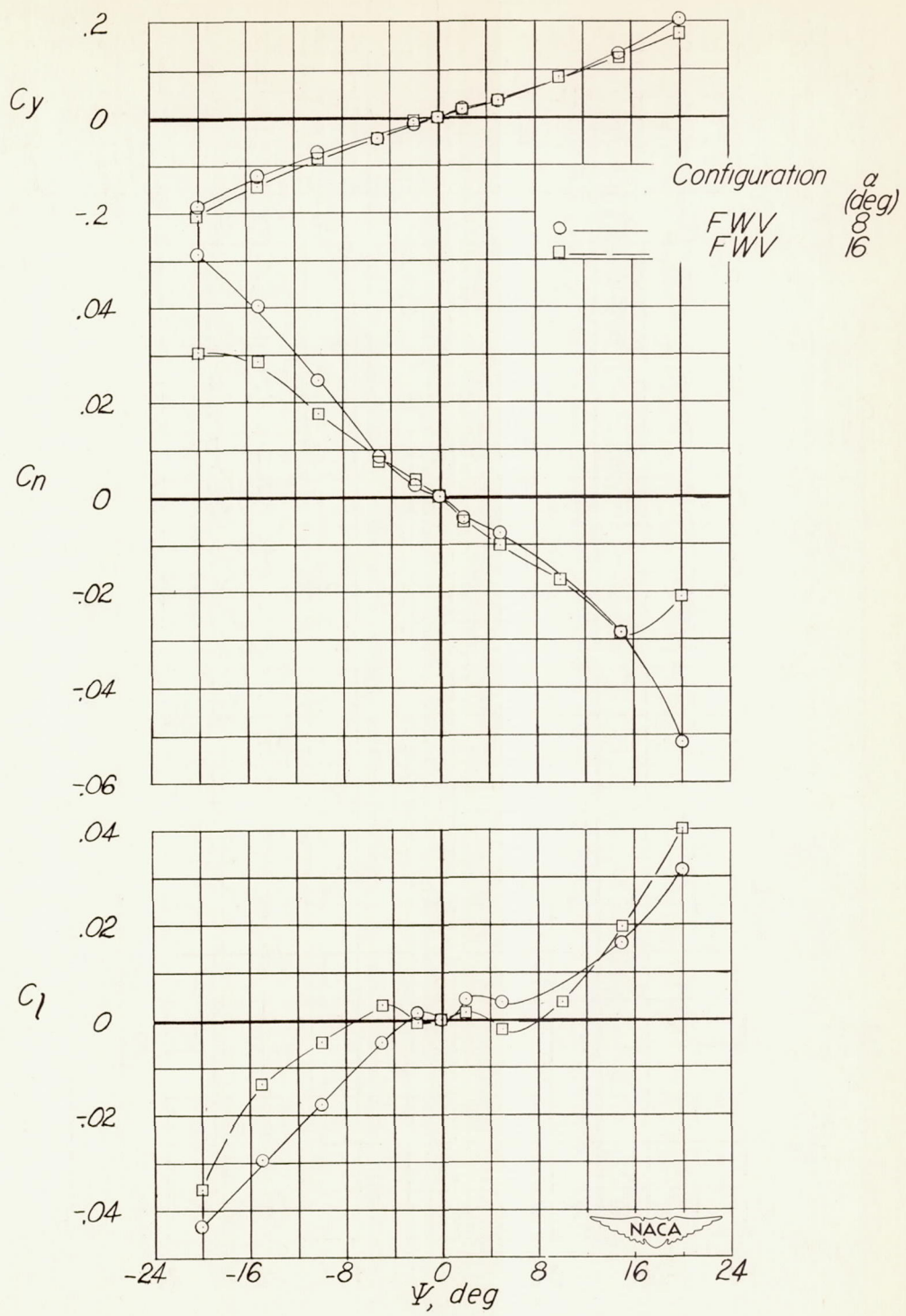
(a) Configuration of fuselage, wing, and vertical tail.

Figure 14.- Lateral characteristics of the model.
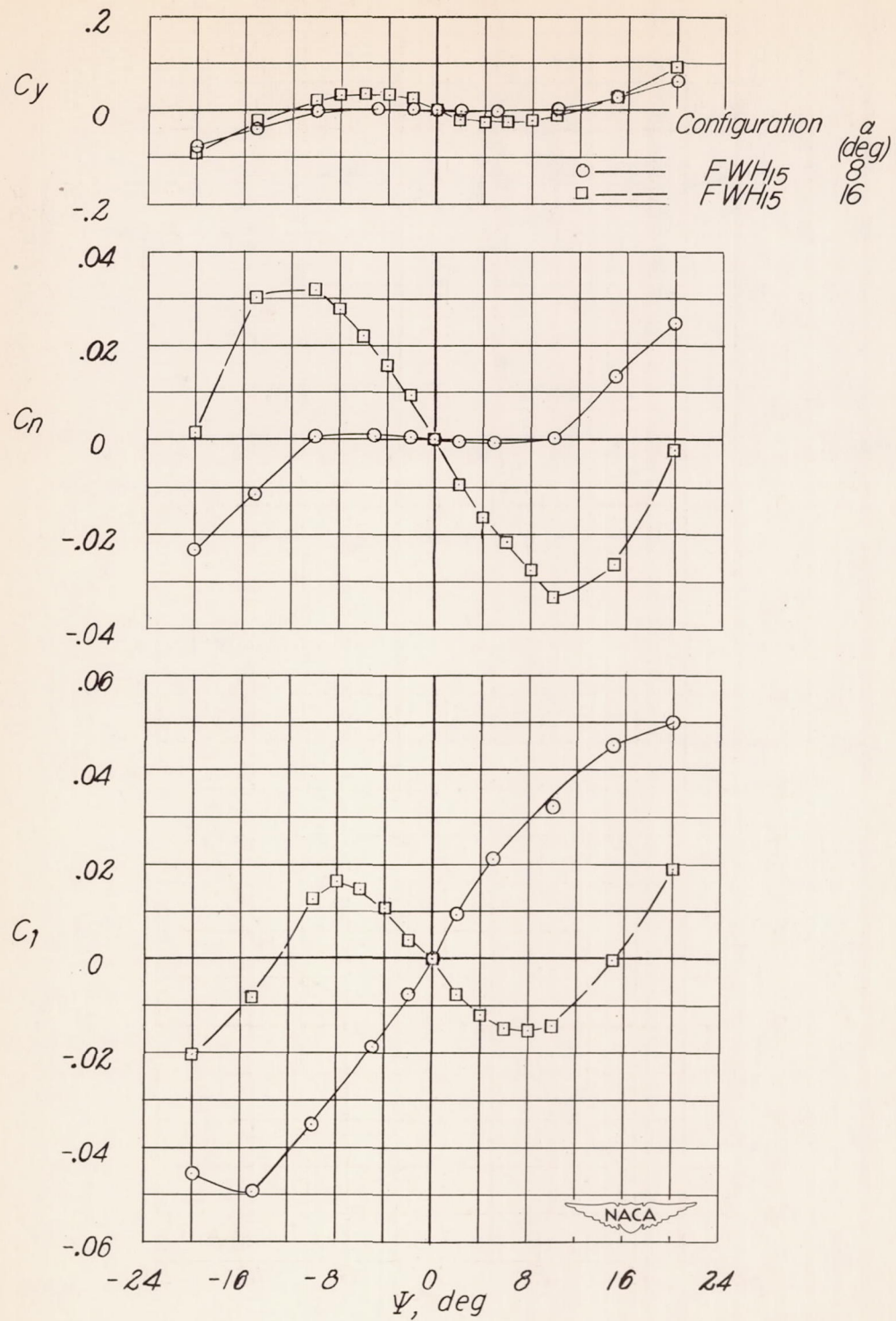
(b) Configuration of fuselage, wing, and horizontal control surface.

Figure 14.- Concluded.
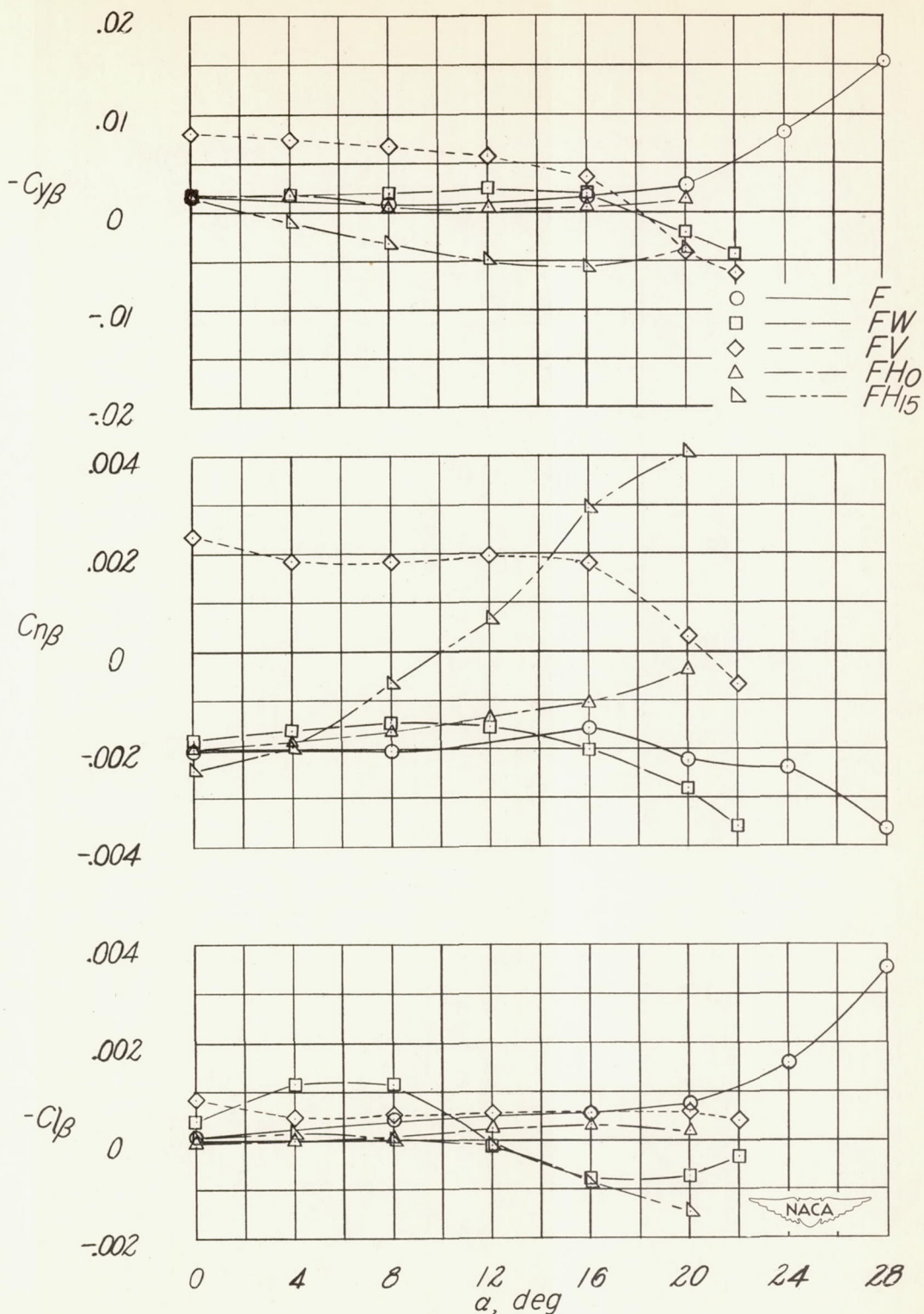
Figure 15.- Lateral stability characteristics of various components in combination with the fuselage.
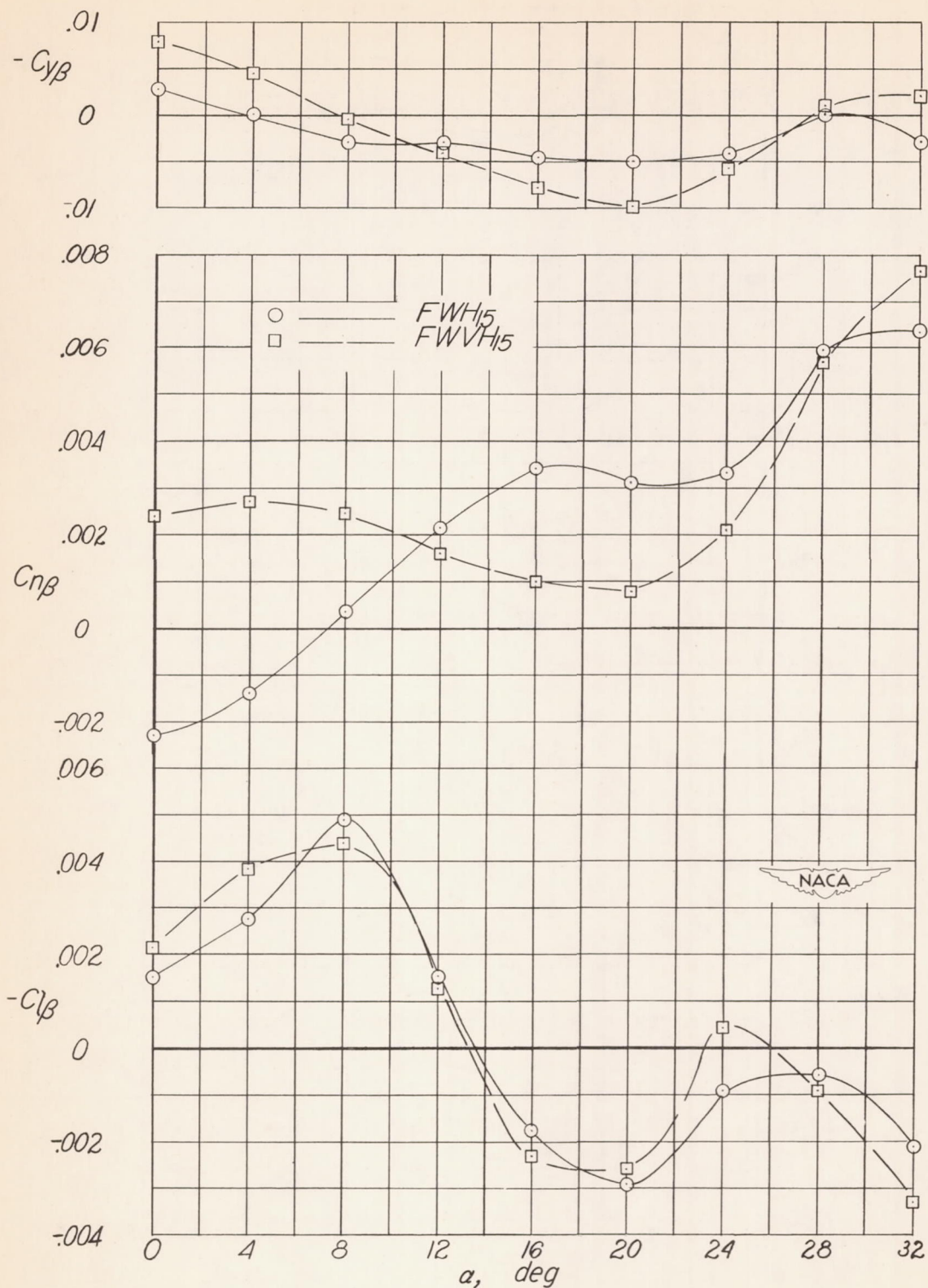
Figure 16.- Lateral stability characteristics of the model up to high angles of attack with vertical tail on and off. $i_t = 15^o$.
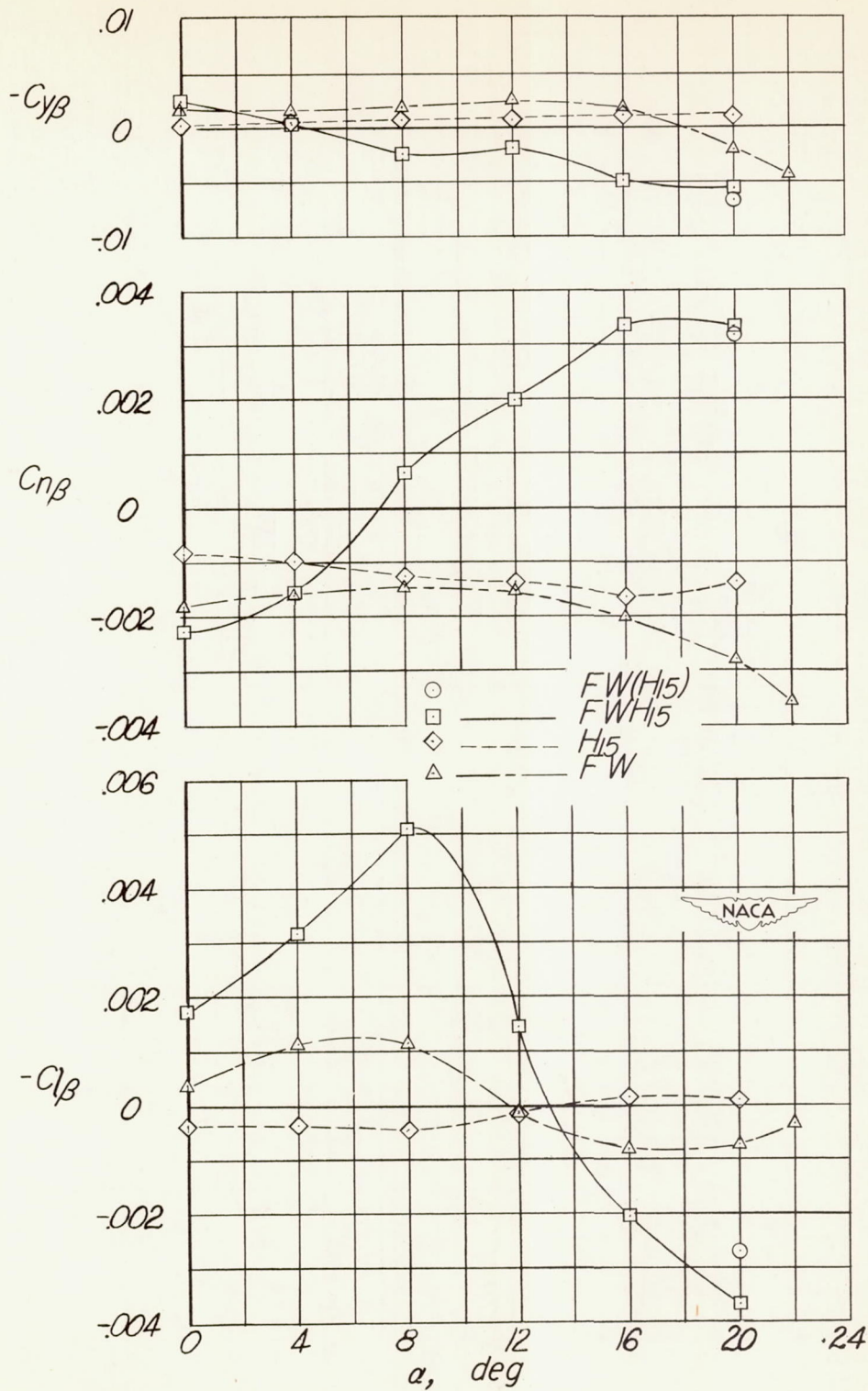
Figure 17.- Comparison of the lateral stability of the model with the
horizontal control surface attached and unattached. Vertical tail off.
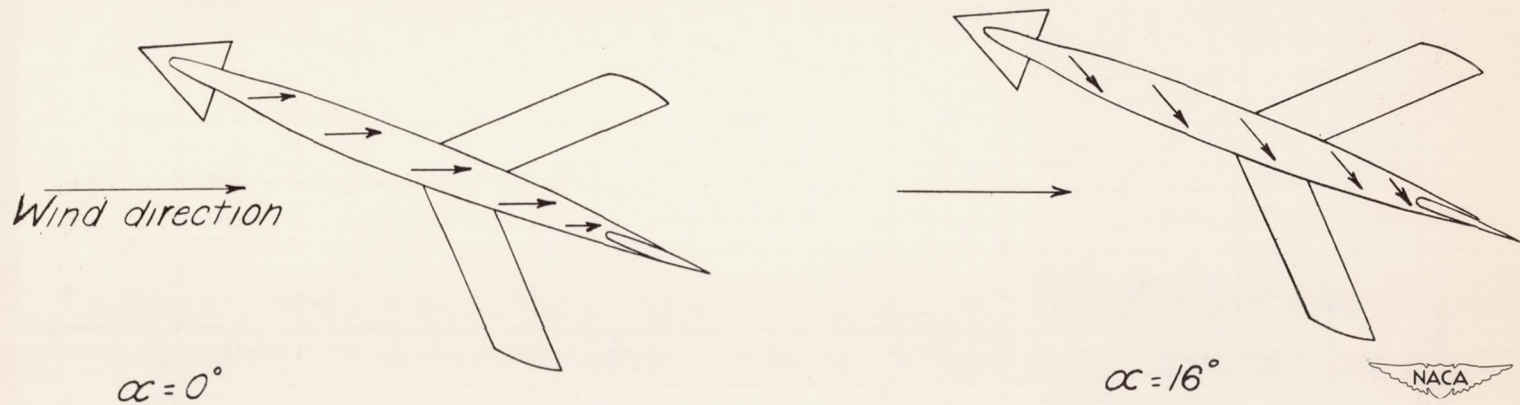
Figure 18.- Direction of air flow over the fuselage for small angles of yaw. $i_t = 15°$.
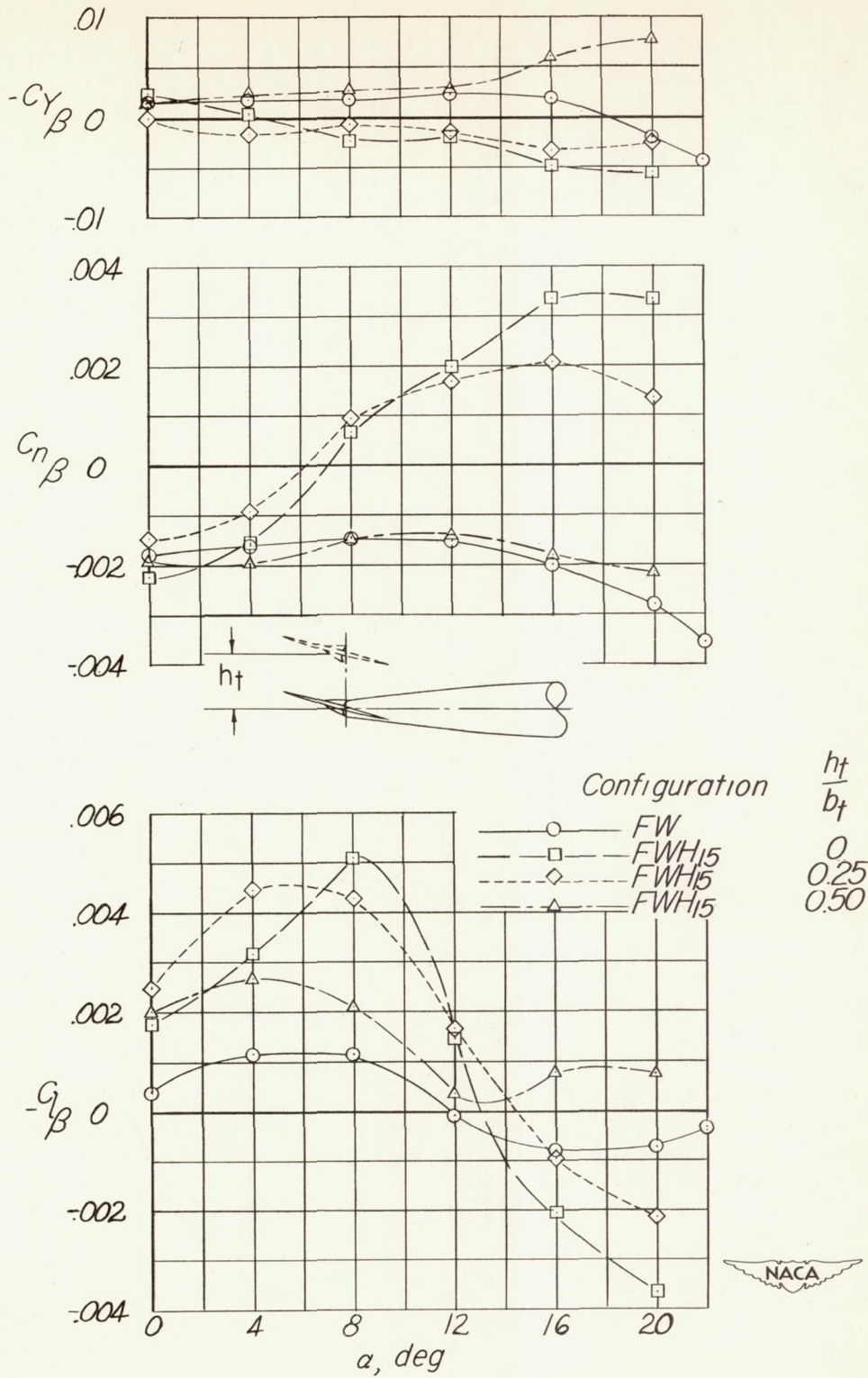
Figure 19.- The effect of vertical location of the horizontal control
surface on the lateral stability characteristics of the model.
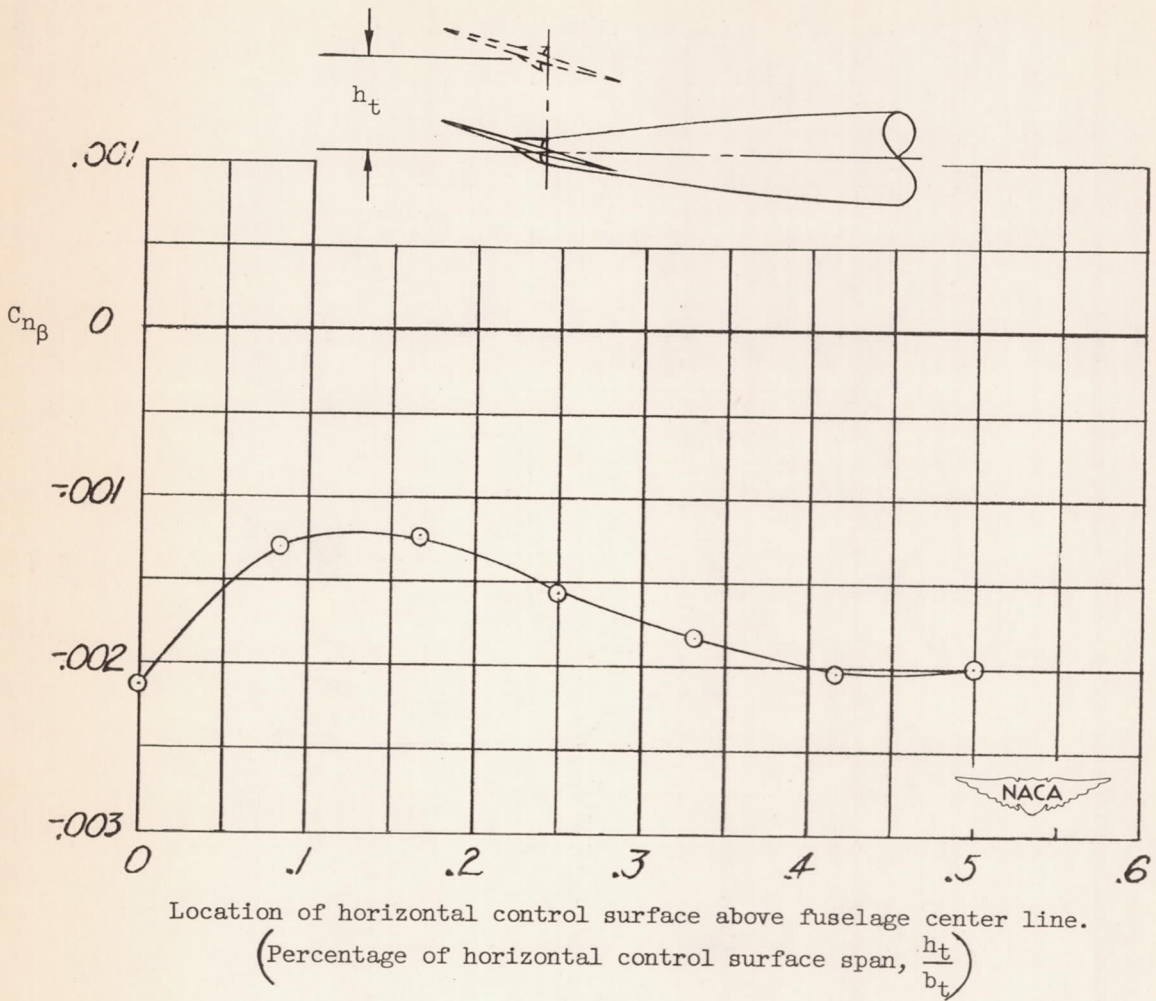
Figure 20.- The effect of vertical location of the horizontal control
surface on the directional-stability parameter of the configuration
of fuselage, wing, and horizontal control surface of the model.
$i_t = 15^o$, $\alpha = 0^o$.
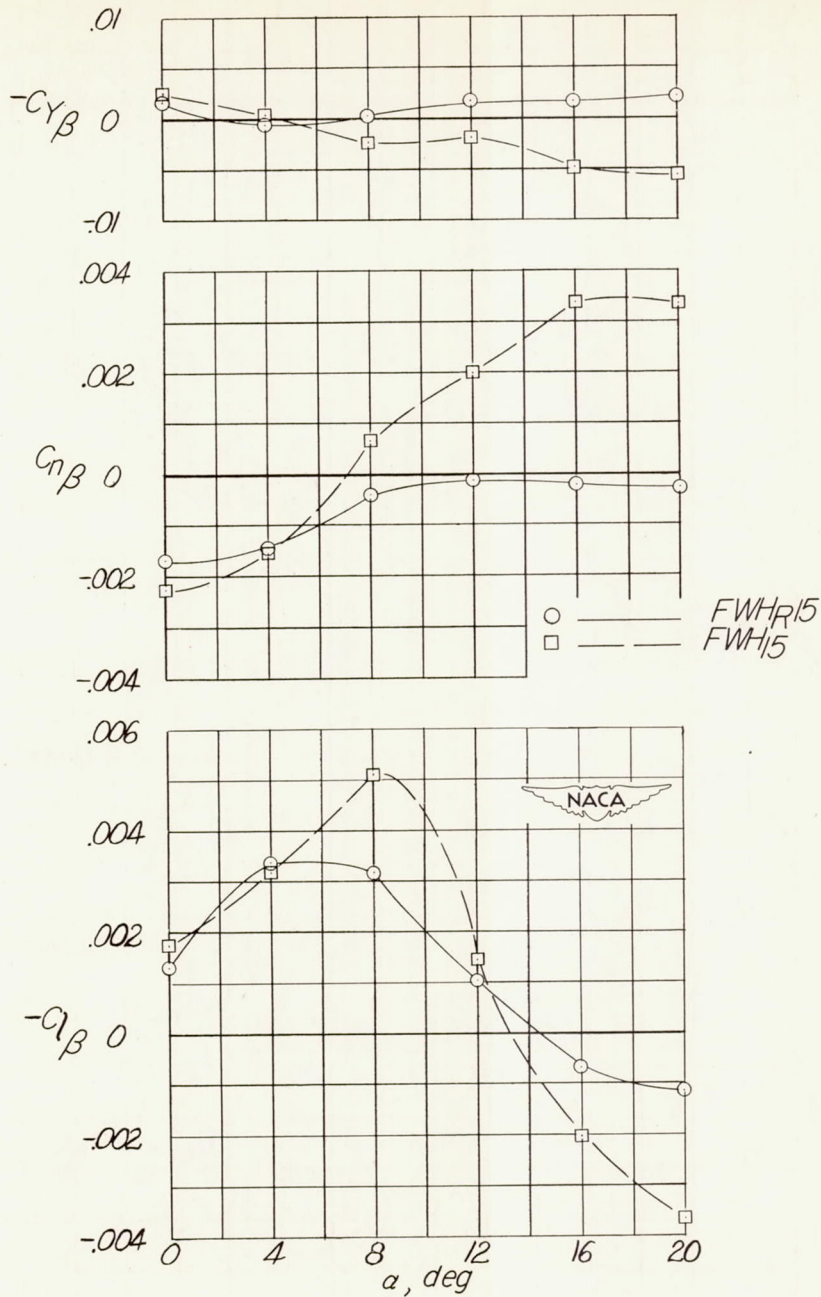
Figure 21.- Comparison of the lateral stability characteristics of rectangular and triangular horizontal-control-surface configurations of the model.
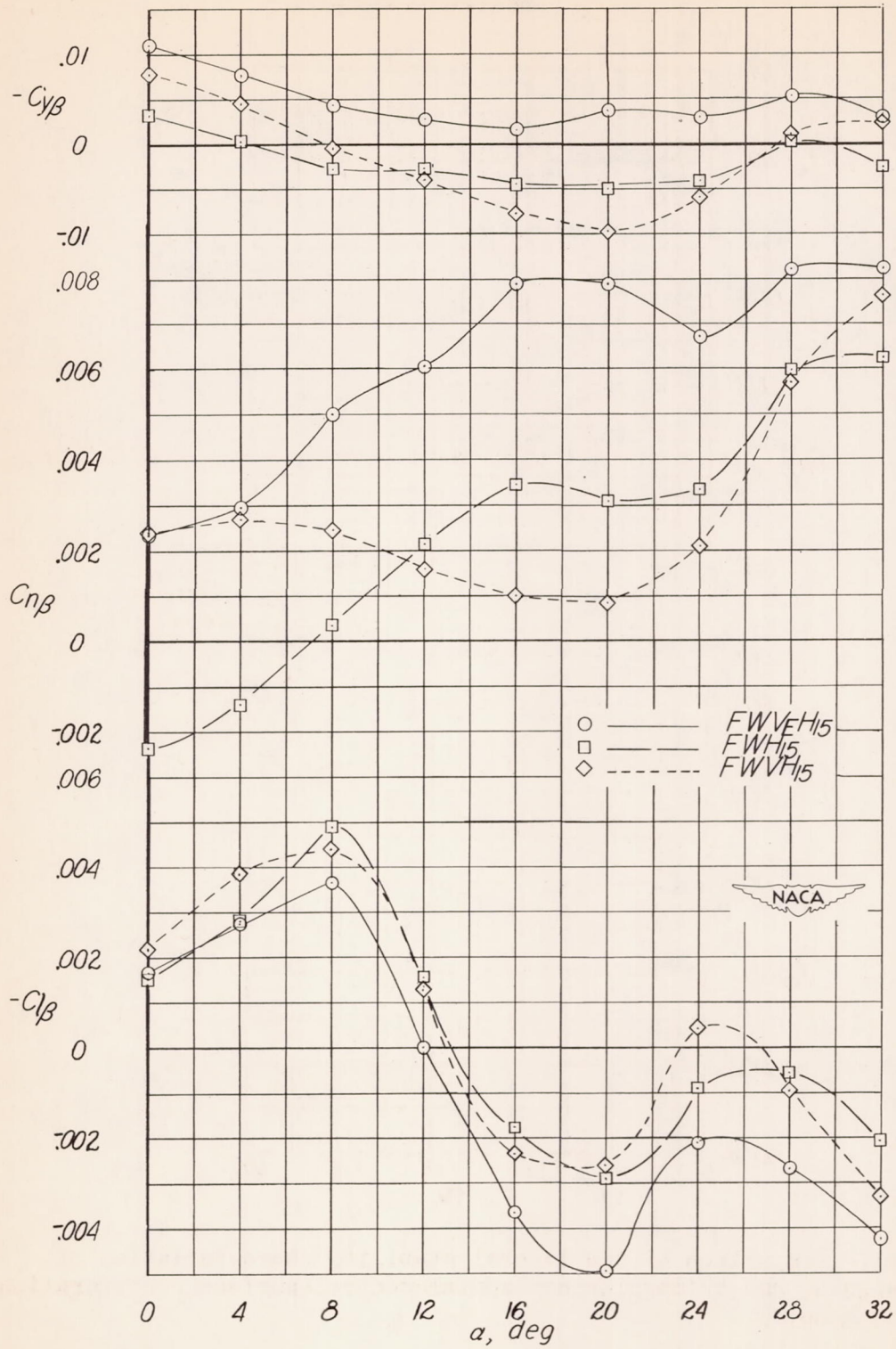
Figure 22.- Comparison of the lateral stability characteristics of single and twin vertical-tail configurations of the model.
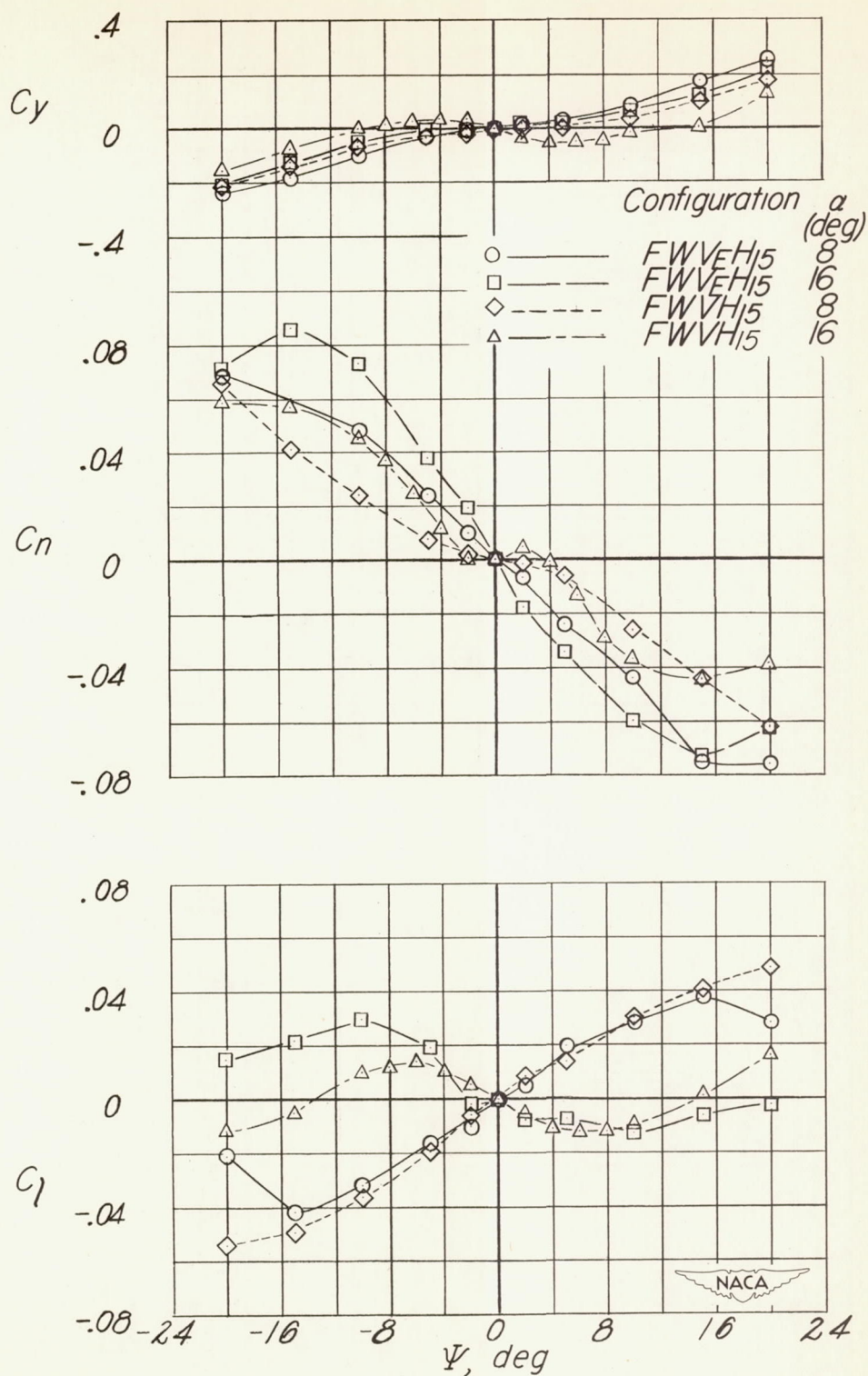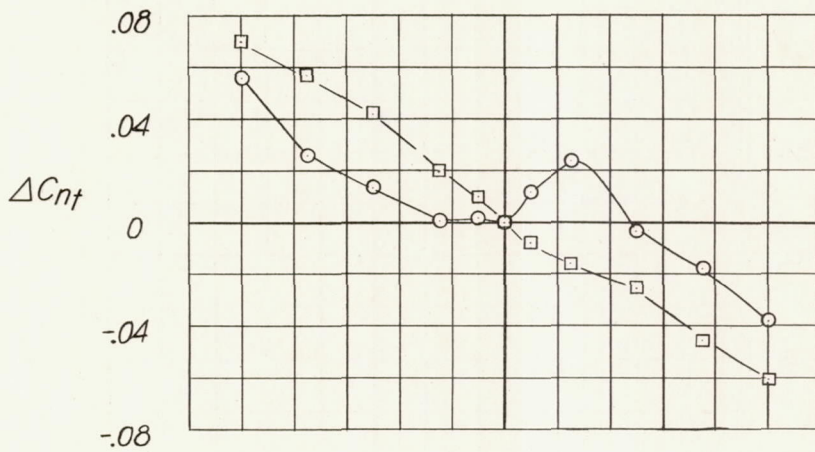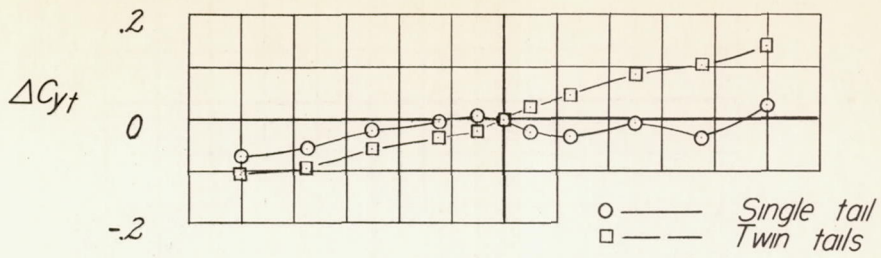
Figure 23.- Lateral characteristics of the model with single and twin
vertical-tail configuration.
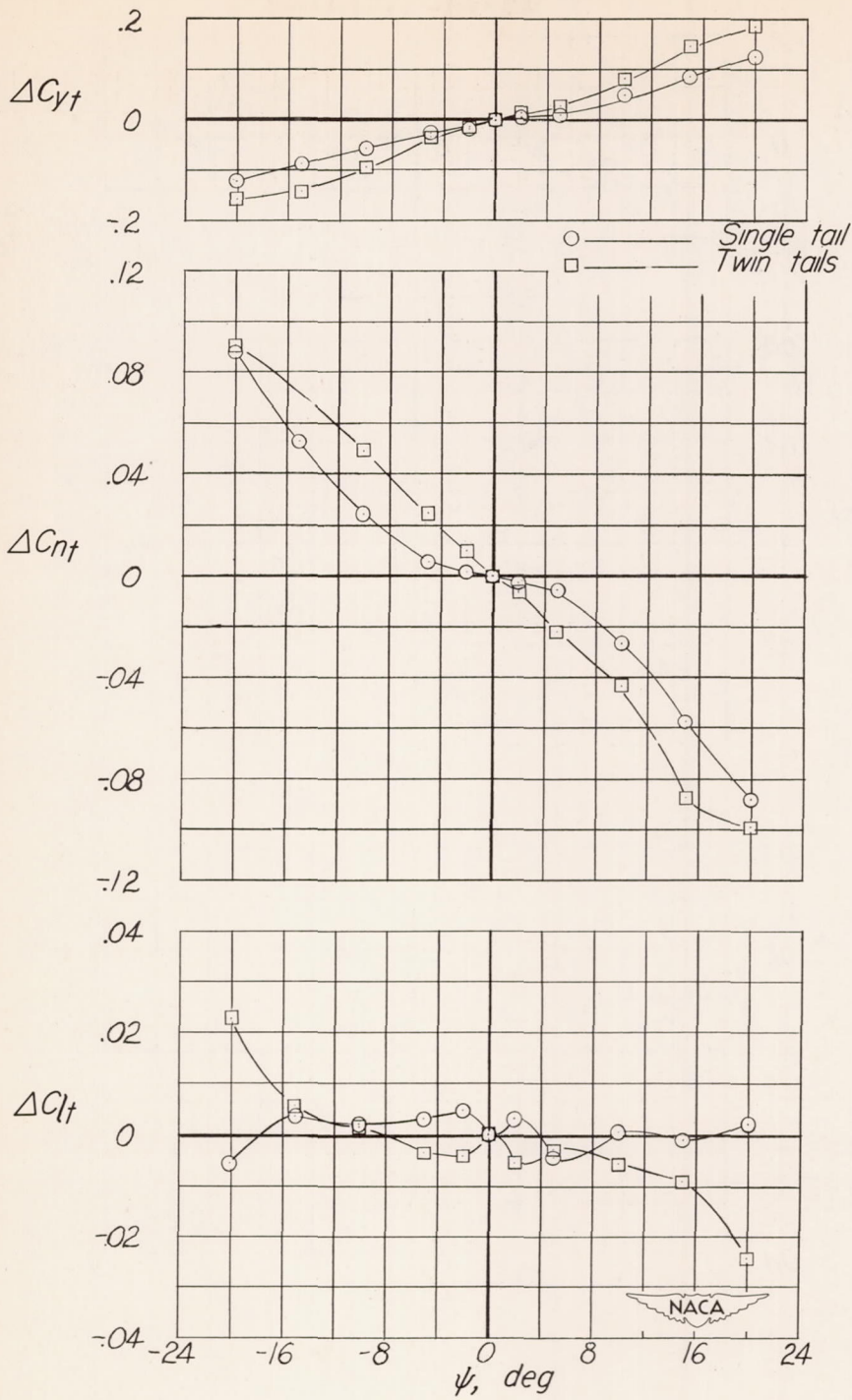
(a) $\alpha = 8°$.

Figure 24.- Incremental lateral stability of single and twin vertical-
tail configurations of the model.
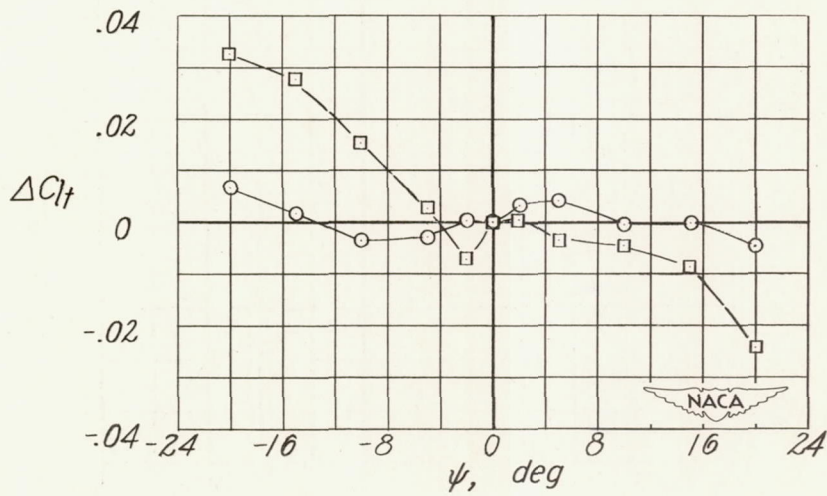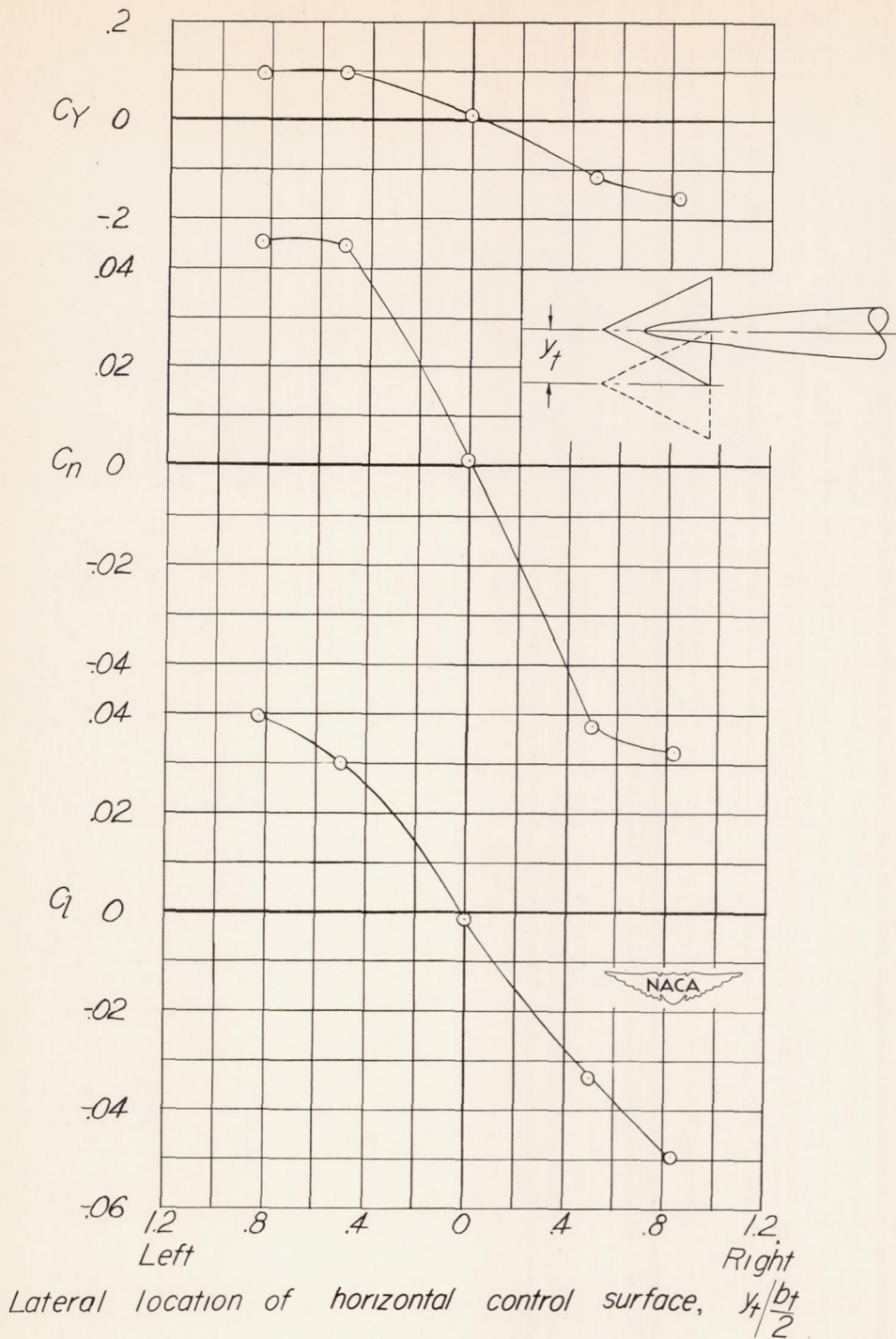
(b) α = 16°.

Figure 24.- Concluded.

Figure 25.- The effect of lateral location of the horizontal control surface on the lateral characteristics of the configuration of fuselage and wing horizontal control surface of the model. $i_t = 15^o$, $\alpha = 15^o$.